British Journal of Pharmacology

DOI:10.1111/j.1476-5381.2011.01780.x
www.brjpharmacol.org

RESEARCH PAPER

Gallium compound GaQ_3-induced Ca^{2+} signalling triggers p53-dependent and -independent apoptosis in cancer cells

Correspondence
Professor Uttam Pati, School of Biotechnology, Jawaharlal Nehru University, New Delhi-110067, India. E-mail: uttam@mail.jnu.ac.in

Keywords
GaQ_3; PARP; ROS; Ca^{2+}; p53

Received
18 May 2011
Revised
31 October 2011
Accepted
31 October 2011

Rajan Gogna[1], Esha Madan[1], Bernhard Keppler[2] and Uttam Pati[1]

[1]*Transcription and Human Biology Laboratory, School of Biotechnology, Jawaharlal Nehru University, New Delhi, India, and* [2]*Institute of Inorganic Chemistry, Vienna University, Vienna, Austria*

BACKGROUND AND PURPOSE

A novel anti-neoplastic gallium complex GaQ_3 (KP46), earlier developed by us, is currently in phase I clinical trial. GaQ_3 induced S-phase arrest and apoptosis via caspase/PARP cleavage in a variety of cancers. However, the underlying mechanism of apoptosis is unknown. Here, we have explored the mechanism(s) of GaQ_3-induced apoptosis in cancer cells, focusing on p53 and intracellular Ca^{2+} signalling.

EXPERIMENTAL APPROACH

GaQ_3-induced cytotoxicity and apoptosis were determined in cancer cell lines, with different p53 status ($p53^{+/+}$, $p53^{-/-}$ and p53 mutant). Time course analysis of intracellular Ca^{2+} calcium release, p53 promoter activation, p53-nuclear/cytoplasmic movements and reactive oxygen species (ROS) were conducted. Ca^{2+}-dependent formation of the p53–p300 transcriptional complex was analysed by co-immunoprecipitation and chromatin immunoprecipitation. Ca^{2+} signalling, p53, p300 and ROS were serially knocked down to study Ca^{2+}–p53–ROS ineractions in GaQ_3-induced apoptosis.

KEY RESULTS

GaQ_3 triggered intracellular Ca^{2+} release stabilizing p53–p300 complex and recruited p53 to p53 promoter, leading to p53 mRNA and protein synthesis. p53 induced higher intracellular Ca^{2+} release and ROS followed by activation of p53 downstream genes including those for the micro RNA mir34a. In $p53^{-/-}$ and p53 mutant cells, GaQ_3-induced Ca^{2+}-signalling generated ROS. ROS further increased membrane translocation of FAS and FAS-mediated extrinsic apoptosis.

CONCLUSIONS AND IMPLICATIONS

This study disclosed a novel mechanism of Ca^{2+}-signalling-mediated p53 activation and ROS up-regulation. Understanding the mechanism of GaQ_3-induced apoptosis will help establish this gallium-based organic compound as a potent anti-cancer drug.

Abbreviations

BrdU, 5-bromo-2′-deoxyuridine; DCFDA, 2′,7′ di-chloro-dihydro-fluorescein-diacetate; GaQ_3, tris(8-quinolinolato)gallium (III)(KP-46); Mn-SOD, manganese superoxide dismutase; MTT, 3-(4,5-dimethylthiazol-2-yl)-2,5-diphenyltetrazolium bromide; NAC, N-acetyl cysteine; PBMC, peripheral blood mononuclear cell; ROS, reactive oxygen species; SA-β-Gal, senescence-associated β-galactosidase; TUNEL, terminal deoxynucleotidyl transferase-mediated dUTP nick end labelling

Introduction

A range of gallium compounds have been investigated in clinical trials against a number of malignancies including lymphomas and bladder cancer (Einhorn, 2003; Straus, 2003; Chitambar, 2004; Jakupec and Keppler, 2004). Gallium nitrate has shown significant anti-tumour activity against non-Hodgkin's lymphoma and bladder cancer (Chitambar

et al., 2007), and induced apoptosis in mantle cell lymphoma cells through increased Bax and reactive oxygen species (ROS), along with down-regulation of cyclin D1 (Joseph *et al.*, 2005). Gallium maltolate, a novel hydroxy-pyrone gallium compound, induced apoptosis and circumvented lymphoma cell resistance to gallium nitrate (Chitambar *et al.*, 2007). Gallium (III) complexes that act as a potent proteasome inhibitors have great potential to be developed into novel anti-cancer drugs (Chen *et al.*, 2007). The gallium (III) complexes of 2-pyridineformamide thio-semicarbazones have been shown to induce cytotoxicity in both malignant glioblastoma cells RT2 ($p53^{+/+}$) and T98 cells (p53 mutant) (Mendes *et al.*, 2009).

Recently, we have successfully assessed the therapeutic potential of an orally bio-available gallium complex, tris(8-quinolinolato)gallium(III) (KP46; here referred to as GaQ_3) against cancer cells in phase I clinical trials (Valiahdi *et al.*, 2009). The effects of GaQ_3 on cancer cells involve S-phase arrest of the cell cycle and apoptosis via activation of caspase-9, cleavage of PARP protein and formation of apoptotic bodies (Valiahdi *et al.*, 2009). However, the mechanism of GaQ_3-induced cell death is unknown. Interestingly, the activity profile of GaQ_3 is distinct from that of inorganic gallium salts, as cells exposed to gallium nitrate displayed increased generation of ROS (Joseph *et al.*, 2005). Inorganic gallium salts interfere with physiological and intracellular procurement of iron, thus causing its depletion (Chitambar *et al.*, 2000). These compounds also interact with iron-dependent proteins like ribonucleotide reductase, prolyl-hydroxylase, transferrin and are effective by inhibiting DNA synthesis and transferrin-mediated endocytosis, ultimately resulting in apoptosis (Zanias *et al.*, 2010).

The widely used anti-cancer drug tamoxifen enhances Ca^{2+} signalling in both breast cancer and several primary glioma cells; increasing both the radius of calcium wave propagation by local stimulation and the amplitude of agonist-induced calcium elevations, while retarding the normalization of cytosolic calcium (Zhang *et al.*, 2000). Ca^{2+}–S100B-mediated regulation of p53 transcriptional activity also provides a link between Ca^{2+} signalling and oncogenic processes in which the tumour suppressor protein p53 plays key roles (Ikura and Yap, 2000).; This was confirmed by the fact that Ca^{2+}-activated RAF/MEK/ERK signalling pathway mediated p53-dependent apoptosis (Li *et al.*, 2005a). Furthermore, the Ca^{2+} binding protein S100A2 binds to the p53 C-terminus in cancer cells, and this interaction was Ca^{2+}-dependent and altered p53 transcriptional activity (Mueller *et al.*, 2005). Patients with p53 deletion exhibit higher serum calcium levels (Chang *et al.*, 2005).

By contrast, the chemotherapeutic drug bleomycin induced transient nuclear accumulation of wild-type p53 and (APO-1/FAS) receptor in HepG2 cells (Muller *et al.*, 1997). A direct correlation between wild-type p53 activity and FAS up-regulation after treatment with ionizing radiation was demonstrated, thus suggesting that post-irradiation FAS up-regulation was dependent on activity of wild-type p53 (Sheard *et al.*, 1997). Regulation of FAS (CD95)-induced apoptotic and necrotic cell death has also been linked to ROS in macrophages (Medan *et al.*, 2005). On the other hand, p53 in mitochondria binds to and inhibits manganese-superoxide dismutase (Mn-SOD), thus playing a direct role in ROS generation and apoptosis (Zhao *et al.*, 2005). Each cellular concentration and distribution of p53 has a distinct cellular function, and ROS acts as both an upstream signal that triggers p53 activation and as a downstream factor that mediates apoptosis (Liu *et al.*, 2008). A microarray analysis of H_2O_2-treated cells identified one-third of the 48 highly H_2O_2-responsive genes as targets of p53 (Desaint *et al.*, 2004).

In this study, we have established the mechanism of action of a novel anti-cancer compound GaQ_3. We have shown that GaQ_3 induced both p53-dependent intrinsic and p53-independent extrinsic pathways of apoptosis in cancer cell. GaQ_3 initiated intracellular release of Ca^{2+} ions in $p53^{+/+}$, p53 mutant and $p53^{-/-}$ cells. In $p53^{+/+}$ cells, intracellular Ca^{2+} stabilized the p53–p300 transcriptional complex followed by p53 transactivation in order to trigger p53-dependent apoptosis, whereas in p53 null and p53 mutant cells, Ca^{2+} signalling increased ROS, which induced FAS membrane translocation and FAS-dependent extrinsic apoptosis.

Methods

Cell culture

Four cancer cell lines (MCF-7, HepG2, PC3, H1299), normal keratinocytes and peripheral blood mononuclear cells (PBMC) were obtained from the National Centre for Cell Science (Pune, India) and were maintained in DMEM. The cells were cultured as monolayers in DMEM supplemented with 10% (v/v) heat-inactivated fetal bovine serum and antibiotics, and incubated at 37°C in a humidified atmosphere of 95% air and 5% CO_2 All the transfections were carried out using effectene transfection reagent (Qiagen, Gaithersburg, MD, USA) according to manufacturer's instructions.

Plasmids and reagents

p53 siRNA, miR-34a and miR-34b/c promoter luciferase constructs were used as previously described byLu *et al.* (2006). p300 siRNA SC-29431-V (Santa Cruz Biotechnology, Santa Cruz, CA, USA) was used for p300 gene silencing. p53 2.5 KB promoter luciferase constructs in pGL2 vector were used to study p53 full promoter activity. The ROS scavenger N-acetyl cysteine (NAC) and the Ca^{2+} quencher TMB8 were purchased from Sigma Aldrich Co. (St Louis, MO, USA) FAS siRNA SR300253 (Origene, Rockville, MD, USA) was used for Fas gene silencing.

Time course analysis

For the various time course studies, five Petri dishes for each time point were used.

Cell proliferation and toxicity assays

Cell proliferation was assayed by the 3-(4,5-dimethylthiazol-2-yl)-2,5-diphenyltetrazolium bromide (MTT) assay performed according to the manufacturer's protocol. The MTT cell proliferation assay kit (catalogue no. 10009365) was obtained from Cayman Chemicals (Ann Arbor, MI, USA). The LDH assay was performed with the LDH cell proliferation assay kit (catalogue no. 10008882; Cayman Chemicals), according to the manufacturer's protocol. DNA synthesis was assayed by the immunofluorescence assay for the detection of

5-bromo-2′-deoxyuridine (BrdU) incorporated into cellular DNA, as described previously (Garcia-Berrocal *et al.*, 2007), and using the *In situ* cell proliferation kit fluos (Roche Applied Science, Indianapolis, IN, USA).

Senescence-associated β-galactosidase (SA-β-Gal) staining

MCF-7 and H1299 cells were stained for SA-β-Gal activity using the senescence detection kit (Cell Signaling Technology, Irvine, CA, USA). Briefly, cells were washed with PBS, fixed for 15 min at room temperature, washed again with PBS and treated overnight at 37°C in SA-β-Gal staining reagent (1 mg·mL^{-1} of X-Gal). Cells were then washed with PBS and images were taken at 200× magnification, with phase-contrast microscopy.

Cell cycle analysis

Cells were collected by centrifugation at 500× *g* at 4°C for 5 min. Cell pellet was re-suspended in 1 mL of cold PBS. Cells were then fixed by adding 4 mL of cold absolute ethanol and stored at –20°C in this fixation buffer until ready for analysis. Fixed cells were then centrifuged (500× *g*, 5 min) and the pellet was re-suspended in 1 mL of PBS. 100 µL of 200 µg·mL^{-1} DNase-free, RNaseA was added to cells and incubated at 37°C for 30 min. Then 100 µL of 1 mg·mL^{-1} propidium iodide (PI) was added and incubated at room temperature for 5–10 min. Finally, the samples were transferred to 12 × 75 Falcon tubes and read on Becton Dickinson (Franklin Lakes, NJ, USA) (LSR) flow cytometer.

Annexin V staining

Becton Dickinson flow cytometer was used to detect the apoptotic cell surface shift of phosphatidylserine by the binding of fluorescein isothiocyanate (FITC)-conjugated Annexin V to the outer membrane of intact cells. Floating cells were collected by centrifugation (500× *g*, 5 min) and these, as well as the attached cells, were washed in PBS (Ca^{2+}- or Mg^{2+}-free)/0.1% EDTA. The attached cells were gently scraped off the dish and centrifuged (500× *g*, 5 min). The pelleted cells were treated with 500 µL binding buffer (Abcam, Cambridge, MA, USA) then 5 µL of Annexin V–FITC, and 5 µL PI (10 µg mL^{-1}) was added. Cells were incubated at room temperature for 5 min. These cells were then filtered (70 µm mesh), to eliminate cell aggregates, and were analysed by flow cytometry.

DNA fragmentation assay

Treated cells (10^6) were lysed in 50 µL of NTE buffer (100 mM NaCl, 40 mM Tris–Cl, pH 7.4, 20 mM EDTA) containing 0.5% SDS. The lysate was heated at 65°C for 10 min to inactivate nucleases and digested by a 2 h treatment with 0.5 mg·mL^{-1} proteinase K followed by a 2 h treatment with 0.2 mg·mL^{-1} RNase A at 50°C. The DNA fragmentation was analysed on a 1.8% agarose gel in the presence of 0.5 µg·mL^{-1} ethidium bromide.

Terminal deoxynucleotidyl transferase (TdT)-mediated dUTP nick-end labelling (TUNEL) assay

TUNEL assay was performed using apop-tag fluorescein *in situ* apoptosis detection kit (Invitrogen, Carlsbad, CA, USA). Briefly, the cell lines were grown on glass-bottomed dishes and treated with GaQ_3 as described above. Cells were first washed in equilibration buffer, treated with TdT enzyme in a humidified chamber at 37°C for 1 h; cells were then washed and treated (room temperature, 30 min) in the dark with fluorescein-conjugated anti-digoxigenin. The washed specimens were counterstained with4′-6-diamidino-2-phenylindole DAPI; 1 µg·mL^{-1}) and visualized with Zeiss Axio vision fluorescent microscope.

Assay for Ca^{2+}mobilization

Ca^{2+} was measured using the cell permeable Ca^{2+}-sensitive fluorescent dye Fluo-3 acetoxymethyl ester (Kowaltowski *et al.*, 1998). Where indicated, BAPTA acetoxymethyl ester (10 µM) was added to the culture medium of cells in 10 cm plastic tissue culture plates for a 1 h exposure prior to the loading procedure with Fluo-3 acetoxymethyl ester. The medium was removed from the tissue culture plates and replaced with 4 µM Fluo-3 acetoxymethyl ester diluted in Krebs–Ringer buffer (KRB) [10 mM D-glucose, 120 mM NaCl, 4.5 mM KCl, 0.7 mM Na_2HPO_4, 1.5 mM NaH_2PO_4 and 0.5 mM $MgCl_2$ (pH 7.4 at 37°C)] (Sigma) for 20 min. The dishes were washed once with 5 mL KRB to remove the residual dye. The cells were harvested by trypsinization, washed in 5 mL of Ca^{2+}-free PBS at 37°C, pelleted by centrifugation (500× *g*, 5 min), re-suspended in 1 mL of Ca^{2+}-free PBS at 37°C and analysed immediately for Fluo-3 fluorescence intensity by flow cytometry.

Luciferase assay

Cells were plated in 35 mm Petri dishes the day before transfection so that they reached 60–80% confluence upon transfection. Reporter plasmids (1.0–1.5 mg·mL^{-1}) were transfected with effectene transfection reagent (Qiagen) according to the manufacturer's instructions. After desired treatment period, the cells were washed in cold PBS three times and lysed with 200 mL of the lysis buffer by a freeze–thaw cycle, and lysates were collected by centrifugation at 3700× *g* for 2 min in a bench top centrifuge. Twenty microlitres of supernatant was used for the assay of luciferase activity using a kit (Promega, Madison, WI, USA) according to the manufacturer's instruction. Luciferase activity of 2.5 kb p53 promoter was assayed using hp53-luc plasmid.

Real-time PCR

Real-time PCR was performed using the 7500 fast real-time system (Applied Biosystems, Alameda, CA, USA) using TaqMan probe (Applied Biosystems) (Lu *et al.*, 2006). Glyceraldehyde-3-phosphate dehydrogenase served as an endogenous control to normalize expression. Each sample was analysed in quadruplicate. Relative expression and standard error were calculated by the supplied fast 7500 real-time system software.

Reverse transcriptase PCR

Cells were lysed in appropriate amount of Trizol (1 mL Trizol per well of a six-well plate for cultured cells). Cells were repeatedly and vigorously pipetted. Cells were then kept at room temperature for 5–10 min, and then 200 µL of chloroform per 1 mL of Trizol was added and mixed thoroughly.

The cells were again left at room temperature for 10 min. Cells were then centrifuged at 3700× *g* at 4°C for 15 min, and the upper aqueous colourless layer was transferred to a fresh Eppendorf tube. To this Eppendorf tube, 75 µL LiCl (lithium chloride) followed by 1 mL chilled EtOH (ethanol) were added and kept at –20°C for 2–3 h. The Eppendorf tube was centrifuged at 3700× *g* for 15 min at 4°C. The supernatant was discarded, and 250 µL of 70% EtOH was added, and the tube was kept at room temperature for 2 min. The tube was again centrifuged at 2500× *g* for 5 min at 4°C. Finally, the supernatant was discarded, and the pellet was re-suspended in RNA grade water till it was completely dissolved. Single-strand c-DNA was synthesized for treatment with sense and antisense primers using revert aid TM h minus first strand cDNA synthesis (Fermentas, Amherst, NY, USA). The resulting cDNA was diluted 1:10 before proceeding with the PCR reaction. PCR was conducted in Mastercycler gradient (Brinkmann Instruments, Inc., Westbury, NY, USA). Each PCR reaction used 50 µL cDNA, 2.5 U Taq polymerase (Eppendorf Scientific, Inc., Ocala, FL, USA), 0.2 mM dNTPs and 0.5 µM primer. PCR products were resolved on 2% agarose gel containing 0.01% (v/v) ethidium bromide and visualized by u.v. illuminator. The size of the PCR amplicon was determined by comparison with 100 bp DNA ladder (Promega). The RT-PCR primers were as follows: β-actin, forward, 5′–ATGAAGTGT GACGTTGACATCCG-3′; reverse, 5′–GCTTGCTGATCCACA TCTGCTG-3′; p53, forward,5 CTGGCCCCTGTCATCTTCT GTC-3′; reverse, 5′–CACGCAAATTTCCTTCCACTCG-3′: FAS, forward, 5′-TTGGTGGACCCGCTCAGTA-3′; reverse, 5′-AAT CTAGCAACAGACGTAAGAACCAG-3′.

Micro RNA (miRNA) measurements using real-time PCR: miRNA expression analysis

TaqMan miRNA assays were used to quantify levels of mature miRNAs, as described previously (Lu *et al.*, 2006). Primary miR-34 transcript levels were determined with the superscript III SYBR green one-step qRT-PCR system (Invitrogen).

Western blotting

Whole-cell lysates were prepared using RIPA buffer [10 mM Tris–HCl (pH 7.4), 150 mM NaCl, 1% NP-40, 1 mM EDTA, 0.1% SDS and 1 mM DTT]. Proteins were resolved by 10% or 12% SDS-PAGE and transferred onto PVDF membranes (Invitrogen). Incubations with primary antibodies were followed by incubations with the appropriate secondary antibodies. To quantify Western blotting signals, densitometry was performed using ImageJ software (Bethesda, MD, USA).

Immunoprecipitation

Cells were washed with PBS, harvested, lysed in radioimmune precipitation buffer (50 mM Tris–HCl, pH 7.4, 150 mM NaCl, 1.0% Triton X-100, 0.1% SDS and 1.0% sodium deoxycholate). The whole cell lysate was pre-cleared, and 1.0 µg of polyclonal antibodies was used for immunoprecipitation. After a 2 h incubation with antibodies, 10 µL of protein A-agarose was added to the lysate and further incubated at 4°C for 4 h. Washing was done twice with Nonidet P-40 buffer (20 mM Tris–HCl, pH 7.4, 100 mM NaCl, 10% glycerol, 1.0% Nonidet P-40 and 1 mM EDTA) and once with radioimmune precipitation buffer. Immunocomplexes were released by the addition of SDS loading dye, boiled for 5 min, centrifuged and loaded to 10% SDS-PAGE. Transfer of proteins to nitrocellulose membrane was done and immunoblotted with target antibodies.

p53 ELISA kit

Pathscan total p53 sandwich ELISA kit was purchased from Cell Signaling Technology. The endogenous p53 level was measured in MCF-7 and HepG2 cells, at different times as indicated. Cells were collected and washed twice with PBS. The cells were lysed and processed for detection of p53 according to the manufacturer's protocol.

DNA damage assay

GaQ_3-induced DNA-damage was quantified with the 'DNA Damage Quantification Kit' (JM-K253-25, MBL International Corporation, Woburn, MA, USA) according to the instruction manual.

ROS measurement

ROS levels were determined by incubating the cells in PBS containing 10 µM 2′,7′ di-chloro-dihydro-fluorescein-diacetate (H-DCFDA; Molecular Probes, Eugene, OR, USA) for 30 min at 37°C. DCFDA was metabolized by non-specific esterases to the non-fluorescent product, 2′,7′-di-chloro-dihydro-fluorescein, which was oxidized to the fluorescent product, DCF, by ROS. The cells were washed twice in PBS, trypsinized, re-suspended in PBS and their ROS content measured, using a Becton Dickinson flow cytometer.

Preparation of nuclear and cytoplasmic extracts

Cells were collected with a rubber policeman and pelleted by centrifugation (500× *g*, 5 min). 200 µL of cytoplasmic extraction reagent (CER-I) according to manufacturer's instructions (#78833; NE-PER nuclear and cytoplasmic extraction kit, Pierce inc.) was added per 20 µL of packed cell volume, and the cell pellet was vortexed for 15 s. Cells were treated in presence of CER I for 10 min, followed by treatment with 11 µL of CER II and were further treated for 1 min. Lysed cells were centrifuged at 4100× *g* for 5 min to pellet the intact nuclei. The supernatant containing the cytoplasmic fraction was carefully separated. The pelleted nuclei were re-suspended in 100 µL of NER I, vortexed for 15 s and treated on ice for 45 min with periodic vortexing after every 10 min. At this point, the suspension was centrifuged (4100× *g*, 5 min) and the supernatant carrying the nuclear proteins was stored at –80°C.

Protein ELISA

The wells of PVC microtitre plate were coated with polyclonal antibodies at a concentration of 1–10 $\mu g \cdot mL^{-1}$ in carbonate/bicarbonate buffer (pH 7.4). The plate was covered with an adhesive plastic and incubated overnight at 4°C. The coating solution was removed, and the plate was washed twice by filling the wells with 200 µL PBS. The solutions were removed by flicking the plate over a sink. The remaining protein-binding sites in the coated wells were blocked by adding 200 µL blocking buffer, 5% non-fat dry milk/PBS, per well. Again, the plate was covered and treated overnight at 4°C. 100 µL of appropriately diluted cell suspension was added to each well and treated for 90 min at 37°C. Diluted monoclonal detection antibody (0.5 µg·in 100 µL) was added to each well.

The plate was covered with an adhesive plastic and incubated for 2 h at room temperature. The plates were washed four times with PBS. 100 µL (containing 0.01 µg) of secondary antibody conjugated with horseradish peroxidase was added to the plate. The plate was covered with an adhesive plastic and treated for 1–2 h at room temperature. The plate was washed four times with PBS.

Chromatin immunoprecipitation

Formaldehyde was added at a final concentration of 1% directly to cell culture media. Fixation proceeded at 22°C for 10 min and was stopped by the addition of glycine to a final concentration of 0.125 M. The cells were collected by centrifugation (500× *g*, 5 min) and rinsed in cold PBS. The cell pellets were re-suspended in swelling buffer [10 mM potassium acetate, 15 mM magnesium acetate, 0.1 M Tris (pH 7.6), 0.5 mM PMSF and 100 ng of leupeptin and aprotinin/mL], incubated on ice for 20 min, and then homogenized (Dounce homogenizer). The nuclei were collected by micro-centrifugation (5000× *g*, 30 min) and then re-suspended in sonication buffer [1% SDS, 10 mM EDTA, 50 mM Tris–HCl (pH 8.1), 0.5 mM PMSF and 100 ng of leupeptin and aprotinin/mL] and incubated on ice for 10 min. Before sonication, 0.1 g of glass beads (212 to 300 µm diameter; Sigma) was added to each sample. The samples were sonicated on ice with an ultrasonic sonicator at setting 10 for six 20 s pulses to an average length of approximately 1000 bp and then micro-centrifuged (5000× *g*, 45 min). The chromatin solution was pre-cleared with the addition of *Staphylococcus aureus* protein A-positive cells for 15 min at 4°C. Prior to use, the Staph A cells were blocked with sheared herring sperm DNA (1 µg μL^{-1}) and BSA (1 µg μL^{-1}) for at least 4 h at 4°C. Pre-cleared chromatin from 10^7 cells was incubated with 1 µg of affinity-purified rabbit polyclonal antibody or no antibody and rotated at 4°C for approximately 12 to 16 h. Before the first wash, 20% of the supernatant from the reaction with no primary antibody for each time point was saved as total input chromatin and was processed with the eluted immunoprecipitates beginning at the cross-link reversal step. Cross-links were reversed by the addition of NaCl to a final concentration of 200 mM, and RNA was removed by the addition of 10 µg of RNase A per sample followed by incubation at 65°C for 4 to 5 h. The samples were then precipitated at –20°C overnight by the addition of 2.5 volumes of ethanol and then pelleted by micro-centrifugation (5000× *g*, 15 min). The samples were re-suspended in 100 µL of Tris-EDTA (pH 7.5), 25 µL of 5 × proteinase K buffer [1.25% SDS, 50 mM Tris (pH 7.5) and 25 mM EDTA], and 1.5 µL of proteinase K (Boehringer Mannheim, Indianapolis, IN, USA) and incubated at 45°C for 2 h. Samples were extracted with phenol–chloroform–isoamyl alcohol (25:24:1) followed by extraction with chloroform–isoamyl alcohol and then precipitated with 1/10 volume of 3 M sodium acetate (pH 5.3), 5 µg of glycogen and 2.5 volumes of ethanol. The pellets were collected by micro-centrifugation (5000× *g*, 10 min), re-suspended in 30 µL of H_2O and analysed by PCR.

Data analysis

Data are shown as means ± SD and differences between group means were assessed with ANOVA. Values of $P < 0.05$ were taken to show a significant difference.

Results

GaQ_3 causes cytotoxicity and cellular senescence in $p53^{+/+}$ and $p53^{-/-}$ cancer cells

GaQ_3 has been previously shown to have anti-proliferative activity in a variety of human cancer cells (Valiahdi *et al.*, 2009). In this study, the role of the p53 tumour suppressor protein in GaQ_3-mediated cytotoxicity and cellular senescence was analysed. The IC_{50} values of GaQ_3 were determined in three types of caner cells; those with normal, wild-type, p53 ($p53^{+/+}$) i.e., MCF-7 and HepG2 cells), those with deletion of p53 ($p53^{-/-}$) i.e., H1299 cells and those with mutant forms of p53 (p53 mutant) i.e., PC3 cells (Figure 1A), using MTT and LDH assays (Figures S1–S6). The IC_{50} values of GaQ_3 for MCF-7, HepG2, H1299 and PC3 cells were 4.1, 4.2, 5.5 and 5.9 µM respectively. A significant difference in the IC_{50} values of $GaQ_{33}$was observed in $p53^{+/+}$, $p53^{-/-}$ and p53 mutant cells (Figure 1A). In non-cancer, control cells, such as normal keratinocytes and normal PBMCs, the IC_{50} was 18 and 16 µM GaQ_3 respectively (Figure 1A). These data show that GaQ_3 is selectively toxic towards cancer cells since the IC_{50} values of GaQ_3 for normal cells were higher than those in the cancer cell lines. To confirm the role of p53 in GaQ_3-induced cytotoxicity, two closely related cell lines, HCT-$p53^{+/+}$ and HCT-$p53^{-/-}$ cells, were used and IC_{50} values of 4.4 µM and 7.78 µM, respectively, were obtained.

The BrdU assay was used to analyse the effect of GaQ_3 treatment on cellular DNA synthesis (Figure 1B) and showed inhibition of DNA synthesis (low BrdU uptake) in GaQ_3-treated MCF-7, H1299 and PC3 cells, whereas the untreated cells did not show any decline in BrdU uptake. This suggested that GaQ_3 abolished DNA synthesis in both $p53^{+/+}$ and $p53^{-/-}$ cells. The SA-β Gal assay (Figure 1C) showed high SA-β Gal staining in GaQ_3-treated cells in MCF-7, H1299 and PC3 cells. We thus concluded that cancer cells with wild-type p53 were more susceptible to GaQ_3; although GaQ_3 was cytotoxic to all three types of cancer cell ($p53^{+/+}$, $p53^{-/-}$ and p53 mutant). Furthermore, GaQ_3 also induced inhibition of DNA synthesis and cellular senescence but this function was independent of p53 status in cancer cells.

GaQ_3 induces G_1/S-phase arrest and apoptosis in cancer cells

The results obtained from the BrdU assay suggested that GaQ_3 might also interfere with cell cycle progression in cancer cells. The cell cycle distribution curve of GaQ_3-treated MCF-7, H1299 and PC3 cells was analysed with PI staining and flow cytometry (Figures 2A and S7). This analysis showed G_1/S-phase arrest and a significant sub-G_1 peak. The G_1–S phase arrest indicated that GaQ_3 might interfere with initiation of DNA replication and synthesis of DNA during S phase. Annexin V staining showed a significant apoptotic fraction in MCF-7 (67%), H1299 (51%) and PC3 (58%) cells after treatment with GaQ_3 (Figures 2B and S8). These data indicated that GaQ_3 induced apoptosis via both p53-dependent and -independent pathways. The nature of cell death (either apoptotic or necrotic) induced by GaQ_3 in cancer cells was examined by inhibiting caspase-3 in the treated cells (Figure S9). Inhibition of caspase-3, using DEVD-FMK, significantly reduced GaQ_3-induced apoptosis, showing that GaQ_3 induced

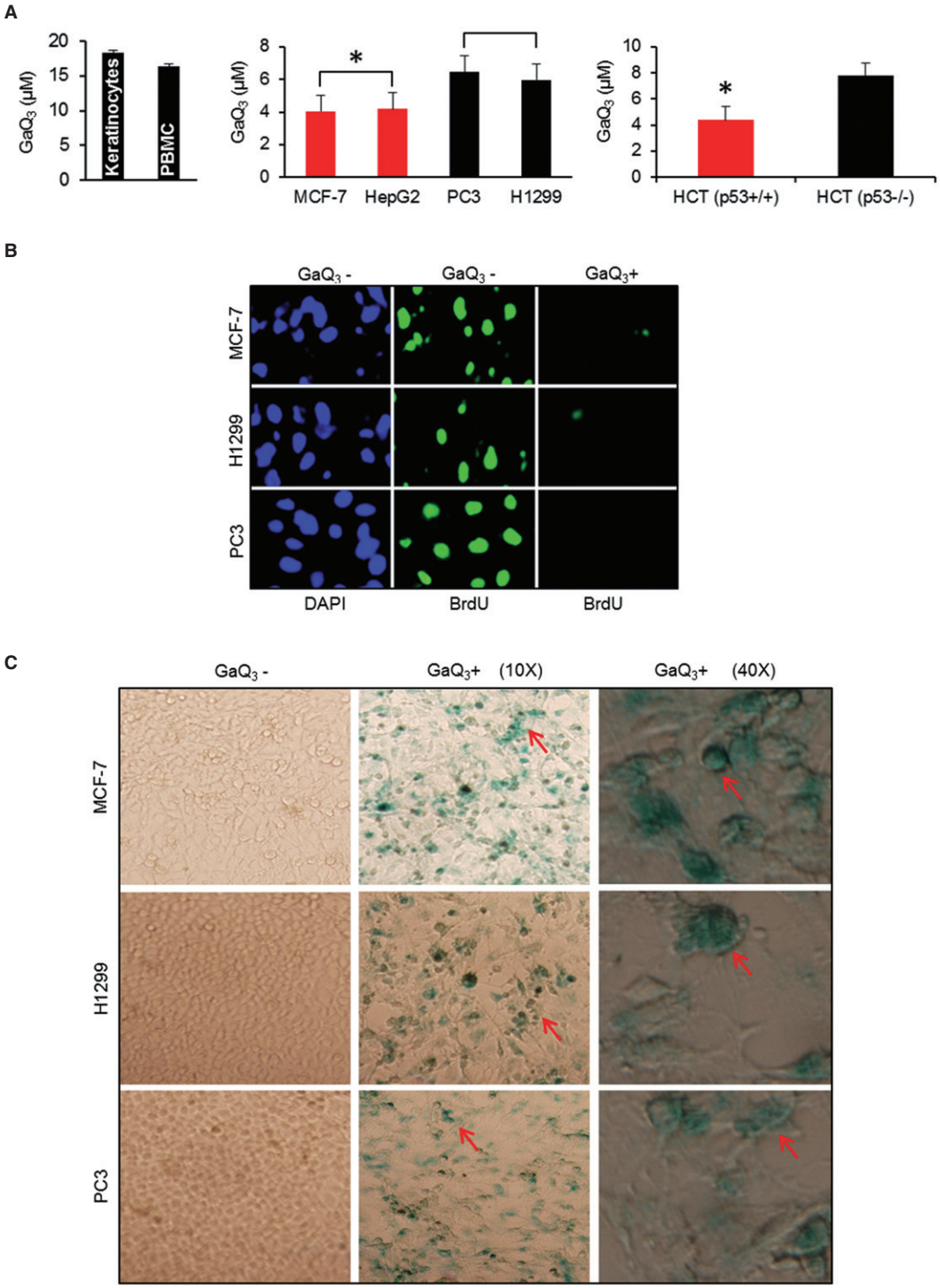

Figure 1

GaQ_3 induces cytotoxicity in $p53^{+/+}$ and $p53^{-/-}$ cells. (A) IC_{50} values of GaQ_3-treated normal keratinocytes and PBMCs are calculated based on MTT and LDH assays. IC_{50} values of GaQ_3 in normal keratinocytes and PBMCs were higher than those in MCF-7, HepG2, PC3 and H1299 cells. In the middle graph, the IC_{50} values are lower for HepG2 cells and $p53^{+/+}$ (MCF-7) cells than in $p53^{-/-}$ (H1299) cells and p53 mutant (PC3) cells. In the last graph the IC_{50} for GaQ_3 in HCT-$p53^{+/+}$ cells was lower than that in HCT-$p53^{-/-}$ cells. Data shown are means ± SD ($n = 10$), $^*P < 0.05$, significant difference between $p53^{+/+}$ and $p53^{-/-}$ or p53 mutant cells; ANOVA. (B) Effect of GaQ_3 on cellular DNA synthesis determined by BrdU assay in MCF-7, H1299 and PC3 cells. Immunofluorescence microscopy was used to visualize BrdU incorporation in control (second panel) and GaQ_3-treated cells (third panel). DAPI was used to stain the nucleus ($n = 7$). GaQ_3 was used for 24 h, at the IC_{50} corresponding to each cell line. (C) $p53^{+/+}$ (MCF-7), $p53^{-/-}$ (H1299) and p53 mutant (PC3) cells were treated with GaQ_3 at corresponding IC_{50}, for 24 h and assayed for cellular senescence using SA-β Gal assay (10× and 40×, phase contrast; $n = 5$).

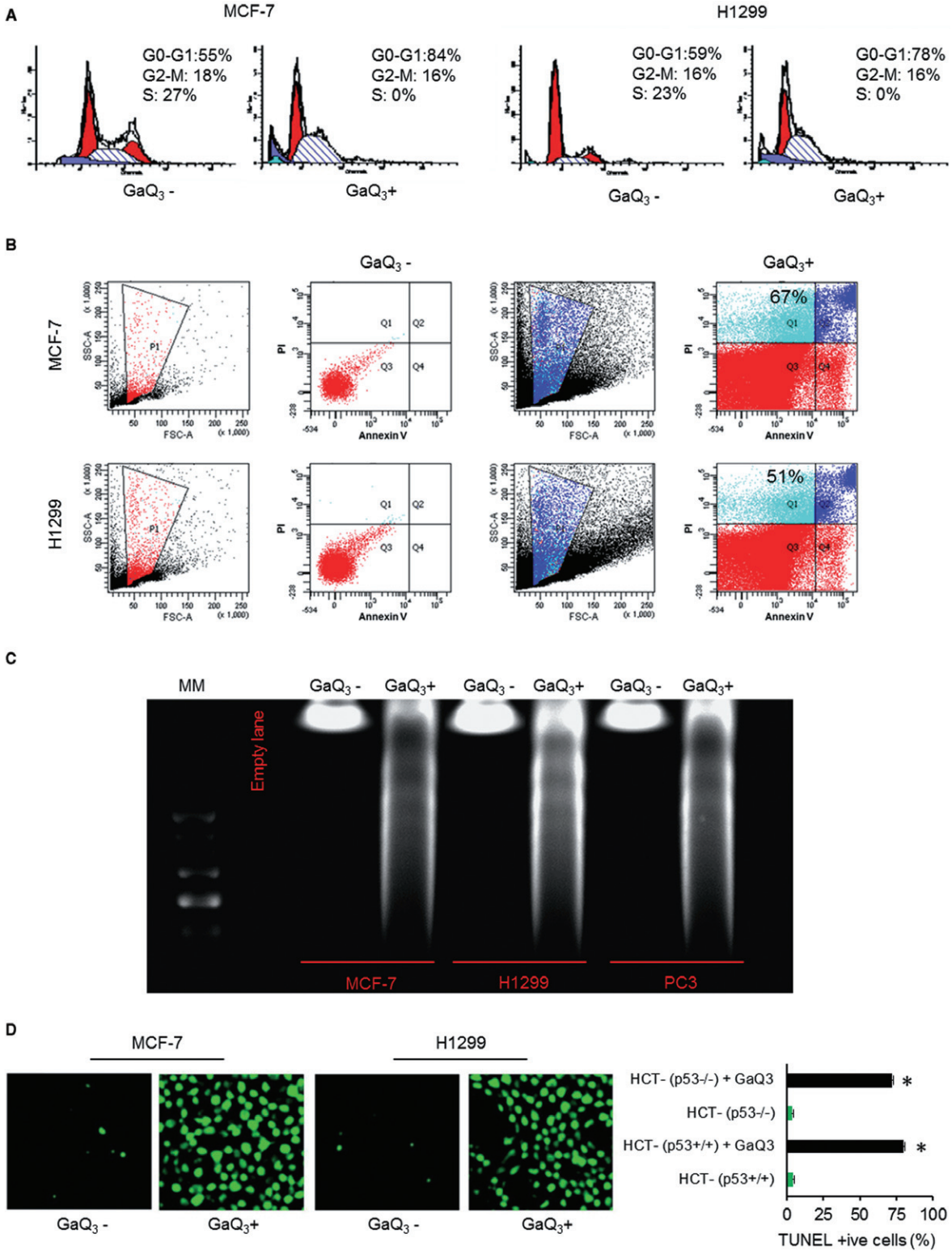

Figure 2

GaQ_3 mediated cell cycle arrest and apoptosis in cancer cells. (A) Effects of GaQ_3 on cell cycle progression in MCF-7 and H1299 cells using PI staining. GaQ_3-treated MCF-7 and H1299 cells show G_1–S phase arrest (n = 10). (B) GaQ_3-induced apoptosis in MCF-7 and H1299 cells using Annexin V-FITC staining, showing 67% and 51% apoptosis, respectively (n = 15). (C) DNA fragmentation assay in GaQ_3-treated MCF-7, H1299 and PC3 cells shows a characteristic DNA ladder indicating GaQ_3-induced apoptosis in all three cell lines (n = 3). (D) TUNEL assay using fluorescence microscopy in MCF-7 and H1299 cells (left panel) and using ELISA-based assays in HCT-$p53^{+/+}$ and HCT-$p53^{-/-}$ cells. In both sets of experiments, GaQ_3-treated cells were TUNEL positive (n = 8).

only apoptotic cell death and not necrosis. DNA fragmentation in GaQ_3-treated MCF-7, H1299 and PC3 cells also showed the typical apoptotic DNA ladder formation (Figure 2C, lanes 4, 6 and 8). TUNEL assay using fluorescence-based and ELISA-based methods showed higher apoptosis in MCF-7, H1299 and PC3 cells (Figures 2D and S10). Fluorescence microscopy-based TUNEL-analysis showed a significant proportion of TUNEL-positive cells after GaQ_3 treatment, whereas 97% of untreated cells were TUNEL-negative. ELISA-based TUNEL assays also showed a significant rise in TUNEL-positive cells upon GaQ_3 treatment in HCT-$p53^{+/+}$, HCT-$p53^{-/-}$ cells (Figure 2D) and MCF-7, H1299 and PC3 cells (Figure S10). These data showed a higher level of apoptotic cells in HCT-$p53^{+/+}$ cultures, again implying an important role of p53 in GaQ_3-induced apoptosis.

GaQ_3 induces intracellular Ca^{2+} release both in $p53^{+/+}$ and $p53^{-/-}$ cells

Metal-based anti-tumour drugs are known to induce Ca^{2+} signalling via intracellular release of Ca^{2+} ions in the cytoplasmic pool (Takemura *et al.*, 1989; Yamagami *et al.*, 1998; Fauskov and Bjerregaard, 2002). We therefore measured intracellular Ca^{2+} release in GaQ_3-treated MCF-7 ($p53^{+/+}$) and H1299 ($p53^{-/-}$) cells using Fluo-3-AM staining and flow cytometry, at different times up to 10 h after GaQ_3 treatment). As shown in Figure 3A, GaQ_3 significantly increased release of intracellular Ca^{2+} within 30 min incubation and a more gradual increase in intracellular Ca^{2+} levels over the next 7–10 h (panels 3 and 4). Interestingly, the 7 and 10 h intracellular calcium levels were 29% higher in MCF-7 cells than in H1299 cells, although the GaQ_3-induced Ca^{2+} release was not totally dependent on p53 status in these cells. A detailed time course analysis showed that GaQ_3 initiated intracellular Ca^{2+} release by 30 min in MCF-7, H1299 and PC3 cells; however, the pattern of Ca^{2+} release between 0 and 24 h was different in $p53^{+/+}$ (MCF-7), $p53^{-/-}$ (H1299) and p53 mutant (PC3) cells (Figure 3B,C). In H1299 (Figure 3B) and PC3 (Figure 3C) cells, intracellular Ca^{2+} increased slowly and gradually over 24 h of incubation. On the other hand, in MCF-7 cells (Figure 3B), there was a substantial burst of intracellular calcium release at 8 h of incubation,. After silencing the p53 gene in MCF-7 cells, GaQ_3-treatment did not induce the 8 h burst of intracellular Ca^{2+} release, although the gradual increase was maintained (Figure 3D). These data suggested that p53 might play a role in regulation of intracellular Ca^{2+} release in cancer cells. The levels of p53 protein, using Western blotting, were significantly increased in GaQ_3-treated MCF-7 cells (Figure 3E). MCF-7 cells treated with p53 siRNA or tamoxifen were used as negative and positive controls respectively.

Stabilization of p53–p300 transcriptional complex and activation of p53 gene in GaQ_3-treated cells

As the p53 protein level was increased in GaQ_3-treated MCF-7 cells and because p53 requires a transcriptional co-activator p300 to form a transcriptional complex and initiate transcription, the effect of GaQ_3 treatment on p53–p300 binding was analysed. As shown in Figure 4A, p53 did not bind to p300 in untreated MCF-7 cells, but upon addition of GaQ_3, p53–p300 binding was observed, suggesting that GaQ_3 treatment up-regulated p53 and stabilized its transcriptional complex with p300. Mdm2 is the known ubiquitin ligase of p53, which participates in p53 degradation and inhibits p53 activity and we looked for an effect of GaQ_3 treatment on p53–mdm2 interactions. In untreated cells (lane 1), p53 and mdm2 were bound together but this complex was broken in presence of GaQ_3 (lane 2). We also assessed the role of Ca^{2+}signalling in p53–p300 binding following GaQ_3 (Figure 4B). As intracellular Ca^{2+} release increased within 30 min of GaQ_3 incubation, MCF-7 cells were treated with GaQ_3 for up to 24 h and the p53–p300 complex assayed at 30 min, 1 h and 3 h. We found p53 bound to p300 at 24 h (also shown in Figure 4A), but not at 30 min or 1 h of GaQ_3 incubation (lanes 4 and 5). Interestingly, at 3 h of GaQ_3 incubation, the p53–p300 complex was stabilized, and after quenching intracellular Ca^{2+} release using TMB-8 (100 μM), this p53–p300 complex was again broken. These data suggested that Ca^{2+} signalling induced binding of p53 to p300 and stabilized the p53 transcriptional complex. We used the non-immunoprecipitated total protein extract (referred to as Input), p53 siRNA and p300 siRNA as controls. As the p53–p300 complex was established, but p53 cellular level was low at the 3 h time point, we hypothesized that this GaQ_3-induced early p53–p300 binding was responsible for up-regulation of p53 mRNA and protein expression. In order to study p53 gene activation by Ca^{2+}-induced p53–p300 complex, we used chromatin immunoprecipitation (Figure 4C) to observe p53 and p300 binding on the p53 minimal promoter (Tripathi *et al.*, 2007) (–157 to –397; upstream of p53 transcription start site). This region of the p53 promoter carries p53 binding sites, and

Figure 3

GaQ_3 induced intracellular release of Ca^{2+} in cancer cells. (A) GaQ_3-induced intracellular Ca^{2+} release in MCF-7 and H1299 cells using Fluo-3-AM dye and flow cytometry, determined after 30 min, 7 h and 10 h of GaQ_3 incubation. Results show increased Ca^{2+} release at 30 min and a slower, maintained, increase over 24 h. MCF-7 cells show higher Ca^{2+} release than H1299 cells (n = 15). (B) Time course of intracellular Ca^{2+} release in GaQ_3-treated MCF-7 and H1299 cells, using flow cytometry. There was a sharp increase in Ca^{2+} release at 8 h in MCF-7 ($p53^{+/+}$) cells, but not in H1299 ($p53^{-/-}$) cells. Data shown are means ± SD (n = 15). (C) Intracellular Ca^{2+} release in p53 mutant (PC3) cells using flow cytometry. Results show a constant increase in intracellular calcium release after GaQ_3 treatment (n = 15, means ± SD). (D) The role of p53 in intracellular Ca^{2+} release in MCF-7 cells analysed by silencing p53 gene using p53 siRNA. Time course of intracellular Ca^{2+} release in GaQ_3-treated MCF-7 cells, with or without p53 siRNA showed that the GaQ_3-induced sharp increase in the intracellular Ca^{2+} release at 8 h was abolished, after p53 gene silencing. Data shown are means ± SD (n = 15). (E) p53 protein level in GaQ_3-treated MCF-7 cells, by Western blot, was increased (lane 2), relative to untreated cells (control). Lanes 3 and 4 show cells treated with p53 siRNA and tamoxifen as negative and positive controls respectively, Tubulin is used as loading control.

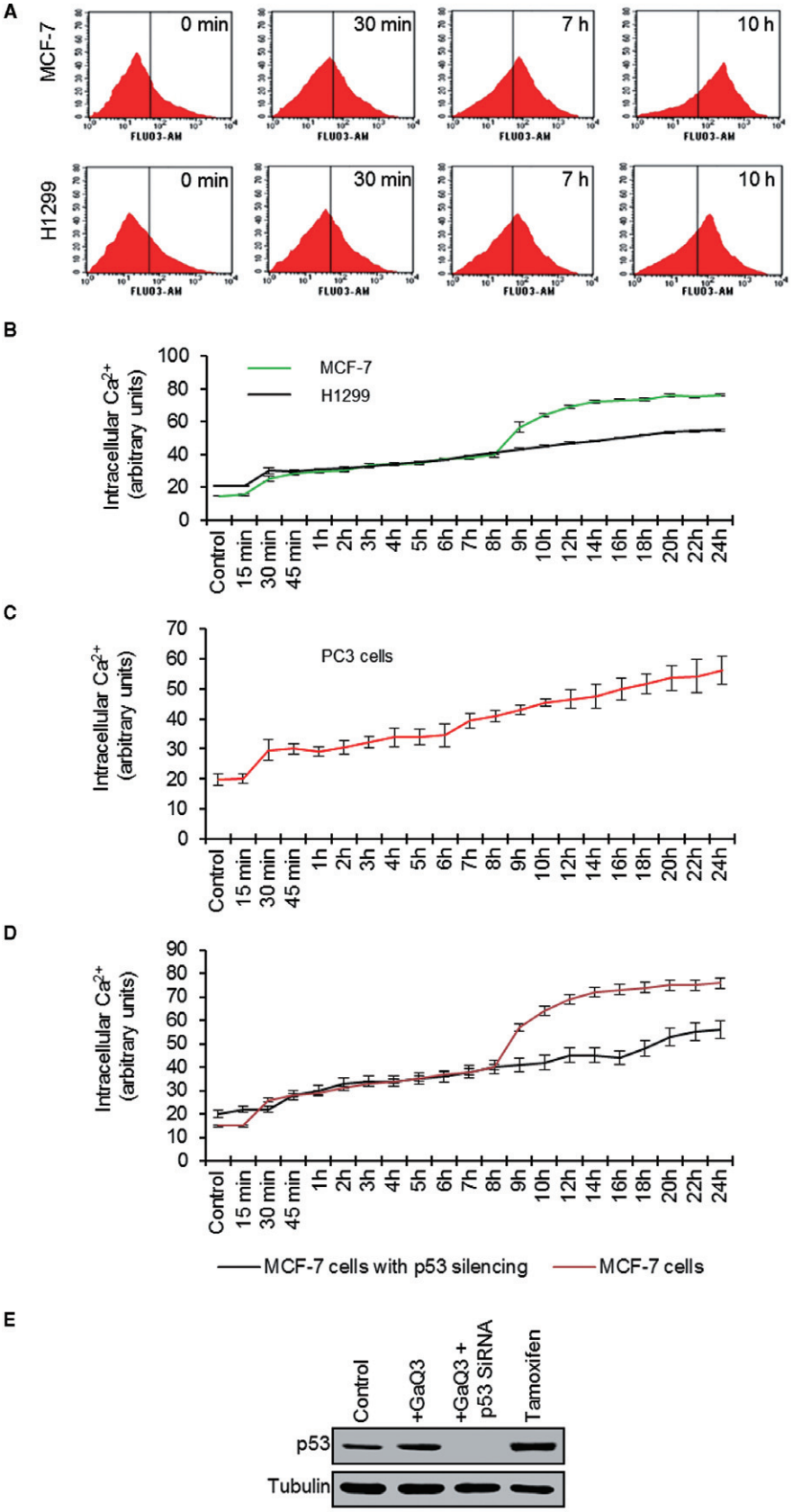
A
MCF-7
H1299
0 min
30 min
7 h
10 h
FLUO3-AM
B
Intracellular Ca2+ (arbitrary units)
MCF-7
H1299
Control
15 min
30 min
45 min
1h
2h
3h
4h
5h
6h
7h
8h
9h
10h
12h
14h
16h
18h
20h
22h
24h
C
PC3 cells
D
MCF-7 cells with p53 silencing
MCF-7 cells
E
Control
+GaQ3
+GaQ3 + p53 SiRNA
Tamoxifen
p53
Tubulin

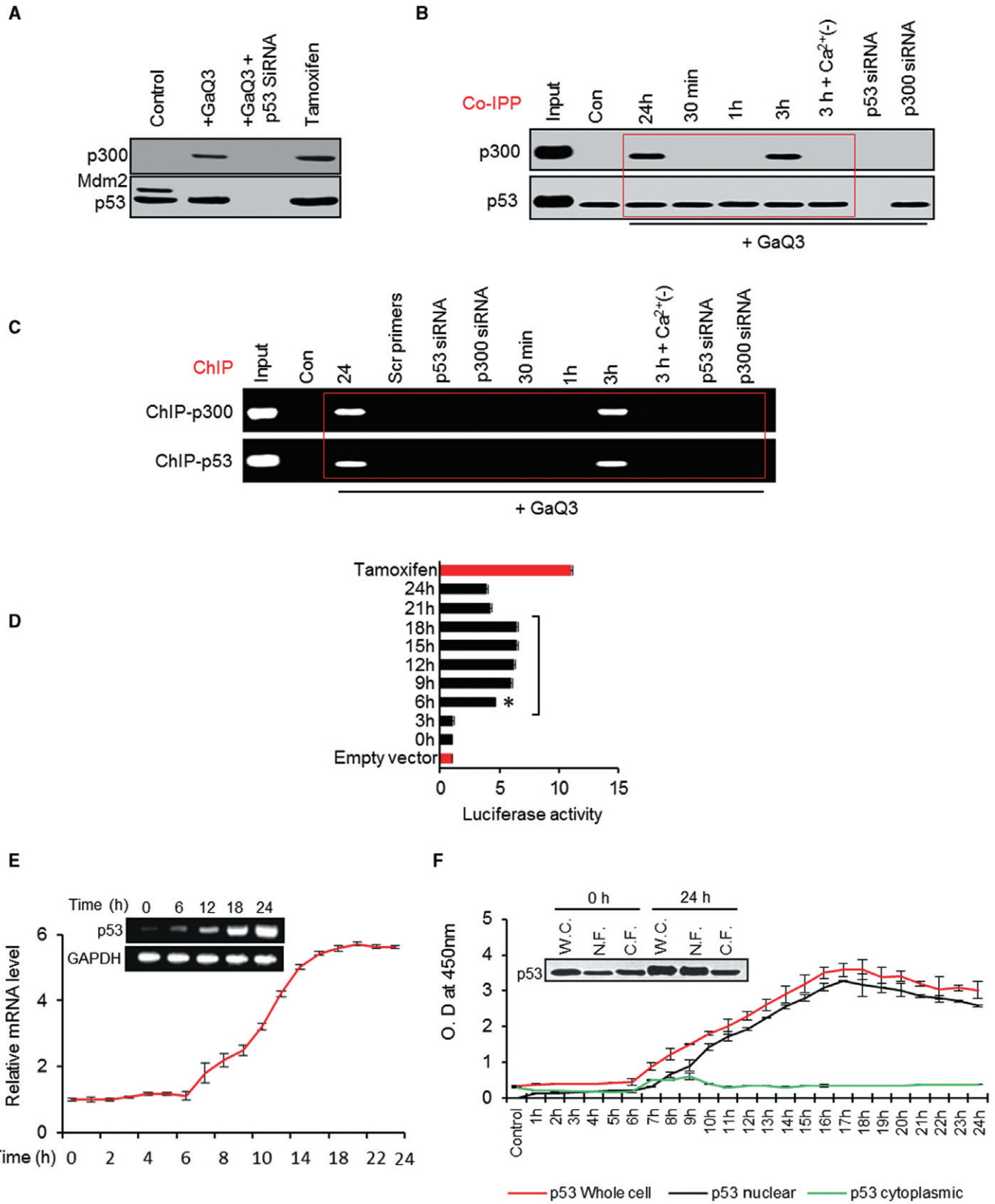
A
Control
+GaQ3
+GaQ3 + p53 SiRNA
Tamoxifen
p300
Mdm2
p53
B
Co-IPP
Input
Con
24h
30 min
1h
3h
3 h + Ca2+(-)
p53 siRNA
p300 siRNA
p300
p53
+ GaQ3
C
ChIP
Input
Con
24
Scr primers
p53 siRNA
p300 siRNA
30 min
1h
3h
3 h + Ca2+(-)
p53 siRNA
p300 siRNA
ChIP-p300
ChIP-p53
+ GaQ3
D
Tamoxifen
24h
21h
18h
15h
12h
9h
6h
3h
0h
Empty vector
*
0
5
10
15
Luciferase activity
E
Time (h) 0 6 12 18 24
p53
GAPDH
Relative mRNA level
0
2
4
6
Time (h) 0 2 4 6 8 10 14 18 22 24
F
0 h
24 h
W.C.
N.F.
C.F.
W.C.
N.F.
C.F.
p53
O. D at 450nm
0
1
2
3
4
5
Control
1h
2h
3h
4h
5h
6h
7h
8h
9h
10h
11h
12h
13h
14h
15h
16h
17h
18h
19h
20h
21h
22h
23h
24h
p53 Whole cell
p53 nuclear
p53 cytoplasmic

Figure 4

GaQ_3 induced p53 expression through Ca^{2+}-mediated stabilization of p5—p300 transcriptional complex. (A) Co-immunoprecipitation (Co-IPP) of p53 with p300 and mdm2 shows p53–p300 binding in GaQ_3-treated cells (lane 2), whereas p53–mdm2 interaction is only observed in untreated cells (lane 1). Tamoxifen (positive control) also induces p53–p300 binding (lane 4) ($n = 10$). (B) The p53–p300 binding is observed in MCF-7 cells after 24 h, 30 min, 1 h and 3 h of GaQ_3 incubation. Results show that p53 binds to p300 at 3 h of GaQ_3 incubation (lane 6). p53–p300 interaction was not observed at 30 min and 1 h of GaQ_3 incubation; however, p53 and p300 were in a complex after treatment with GaQ_3 for 24 h (Figure 3C, as well). Quenching the release of intracellular Ca^{2+} using TMB-8 (100 μM) abolishes the p53–p300 binding induced upon 3 h of GaQ_3 incubation (lane 7). p53 siRNA and p300 siRNA are used as controls (lanes 8 and 9). In this experiment, immunoprecipitation used an anti-p53 N-terminus antibody (Ab421), and Western blots were developed using both anti-p53 and anti-p300 Abs ($n = 8$). (C) The binding of p53–p300 complex to the p53 minimal promoter at 30 min, 1 h and 3 h of GaQ_3 incubation (lanes 7, 8 and 9). Chromatin immunoprecipitation (ChIP) shows strong binding of both p53 and p300 on the –157 to –397 base pairs of p53 minimal promoter in MCF-7 cells treated with GaQ_3 for 24 h (lane 3). No binding of either p53 or p300 was observed at 30 min and 1 h of GaQ_3 incubation (lanes 7 and 8); however, the binding was present at 3 h (lane 9). Upon quenching of intracellular Ca^{2+} release using TMB-8, the GaQ_3-induced p53–p300 binding on p53 minimal promoter is abolished (lane 10) ($n = 8$). p53 and p300 did not show binding to the p53 minimal promoter in the untreated cells (lane 2). The non-immunoprecipitated total protein extract (Input), scrambled primers, p53 siRNA and p300 siRNA are used as controls. (D) The activity of p53 2.5 Kb promoter analysed in GaQ_3-treated MCF-7 cells over 24 h. Results show a significant increase in p53 2.5 Kb promoter activity at 6 h of GaQ_3 incubation. Furthermore, a rise in the promoter activity was observed until 18 h of incubation (*$P < 0.05$, for values from 6–18 h, $n = 4$, means ± SD, ANOVA). (E) p53 mRNA level was determined by real-time PCR in GaQ_3-treated MCF-7 cells in a time-dependent manner (every hour). Results show a significant increase in p53 mRNA level from 6 h of GaQ_3 incubation. ($n = 6$, means ± SD). The mRNA expression is also analysed using RT-PCR at 0, 6, 12, 18 and 24 h of GaQ_3 incubation (inset) ($n = 4$). (F) Time-dependent analysis of the increase in p53 protein expression and p53 nuclear translocation in GaQ_3-treated MCF-7 cells. ELISA using p53 whole cell, nuclear and cytoplasmic fractions show a significant increase in p53 protein level and p53 nuclear translocation at 6 h of GaQ_3 incubation ($n = 8$, SD, ANOVA). Furthermore, the p53 nuclear translocation is confirmed by immunoprecipitation experiment using anti p53 C-terminus antibody (421) in GaQ_3-treated MCF-7 cells at 0 and 24 h time points (WC: whole cell, NF: nuclear fraction, CF: cytoplasmic fraction) ($n = 6$).

p53–p300-mediated activation of this promoter would increase p53 mRNA and protein level. Results showed that both p53 and p300 were bound to the same site as a complex on the p53 minimal promoter after 24 h of GaQ_3 incubation (Figure 4C, lane 3). Interestingly upon p53 silencing, both p53 and p300 did not show binding to the p53 minimal promoter (lane 5). Upon silencing of p300 using p300 siRNA, the binding of both p53 and p300 at the p53 minimal promoter was abolished, suggesting that both p53 and p300 are crucial for the GaQ_3-induced activation of p53 minimal promoter (Figure 4C, lane 6). p53 and p300 both did not bind at the p53 minimal promoter after 30 min and 1 h of incubation with GaQ_3. At 3 h of GaQ_3 incubation, both p53 and p300 showed binding at the p53 minimal promoter, which was abolished after Ca^{2+} quenching (lane 10). Upon silencing both p53 and p300 using their respective siRNAs (Figure 4C, lanes 11 and 12), the 3 h binding of both p53 and p300 to the minimal promoter was abolished. These data suggested that Ca^{2+} signalling induced binding or p53 to its co-activator p300 and then recruited this complex to the p53 minimal promoter to induce up-regulation of p53 gene and protein. Furthermore, the effect of p53–p300 binding to the p53 minimal promoter was assayed by analysing activation of the p53 full (2.5 kb) promoter (Figure 4D). The time course of p53 2.5 kb promoter activity was followed, using the luciferase assay on GaQ_3-treated MCF-7 cells. GaQ_3 activated the p53 promoter at 6 h post GaQ_3 treatment followed by a constant increase in the luciferase activity until 8 h. Ca^{2+} quenching reversed p53 promoter activity in GaQ_3-treated MCF-7 cells (Figure S11). As GaQ_3 induced the p53 minimal promoter by stabilizing the p53–p300 complex, the role of p300 in activation of the p53 promoter was assessed by p53 minimal promoter luciferase analysis in GaQ3-treated MCF-7 cells with p300 silencing (Figure S12). p53 mRNA levels in GaQ_3-treated MCF-7 cells were analysed using both real-time and RT-PCR assay (Figure 4E, RT-PCR in inset). p53 mRNA was increased at 6 h in GaQ_3-treated cells and Ca^{2+} quenching reversed p53 mRNA levels (Figure S13). Furthermore, both p53 mRNA and protein synthesis were reversed in GaQ3-treated cells after p300 gene silencing (Figure S14). These data confirmed the role of calcium-induced p53–p300 complex in p53 up-regulation via activation of the p53 minimal promoter. The time course of increased p53 levels and p53 nuclear translocation was followed in cytoplasmic and nuclear fractions of GaQ_3-treated MCF-7 cells, using immunoprecipitation and *in vivo* ELISA with anti-p53 antibodies (Figure 4F, IPP in inset) and showed significantly increased p53 protein level and p53 nuclear translocation at 9 h of treatment. The purity of nuclear and cytoplasmic fractions was checked by the absence of tubulin in the nuclear fractions (Figure S15, lane 2), and the absence of PARP in the cytoplasmic fractions (lane 3), using immunoprecipitation (Figure S15). The non-immunoprecipitated total protein extract (Input) was used as the control (Figure S15, lane 1).

GaQ_3 damaged DNA in treated cells and DNA damage and p53 stabilization are directly linked (Campaner *et al.*, 2011). In order to establish the role of calcium in stabilization of p53 and to exclude the possibility of DNA-damage-induced p53 activation in GaQ_3-treated cells, the time course of cellular DNA damage was analysed in GaQ_3-treated MCF-7, H1299 and PC3 cells (Figure S16), using apurinic/apyrimidinic (AP) sites as the measure of cellular DNA damage. GaQ_3 treatment did not induce any DNA damage till 15 h of incubation, whereas Ca^{2+}-induced stabilization of p53–p300 complex was present at 3 h and p53 stabilization and up-regulation occurred 6–8 h after GaQ_3 incubation. Thus, GaQ_3-induced DNA damage had no role in p53 up-regulation and p53 gene transcription was up-regulated in MCF-7 cells due solely to GaQ_3-induced intracellular Ca^{2+} release.

Intracellular Ca^{2+} release induces ROS signalling in GaQ_3-treated cells

Ca^{2+} signalling induced ROS in cancer cells (Lemarie *et al.*, 2004; Son *et al.*, 2010) and we analysed the effect of GaQ_3 on cellular ROS, using DCFH-DA staining and flow cytometry (Figures 5A and S17). GaQ_3 induced cellular ROS in MCF-7, PC3 and H1299 cells, although the ROS levels in MCF-7 cells (panel 1) were nearly twofold higher than in H1299 cells (panel 2) and PC3 cells (Figure S18). GaQ_3-induced ROS was independent of p53 status since ROS was up-regulated in both $p53^{+/+}$ (MCF-7) and $p53^{-/-}$ (H1299) cells. However, in MCF-7 cells, p53 gene silencing using p53 siRNA significantly decreased cellular ROS. This suggested that GaQ_3 might initiate ROS synthesis in a p53-independent manner, but the presence of p53 in MCF-7 cells appeared to play a role in amplifying the cellular ROS response (Figure 5A). As p53 was not required for ROS generation in GaQ_3-treated MCF-7 and H1299 cells, we searched for the cellular factors that might be responsible for ROS, by conducting a flow-cytometry-based, time course analysis of ROS level in MCF-7, H1299 and PC3 cells (Figures 5B and S18). Interestingly, the ROS profile in MCF-7 and H1299 cells synchronized with the intracellular Ca^{2+} release profile. Quenching intracellular Ca^{2+} (using TMB-8; 100 μM) in MCF-7 cells led to inhibition of ROS, implying Ca^{2+}-mediated activation of ROS in GaQ_3-treated cancer cells.

Because Ca^{2+} signalling induced both ROS and p53, and ROS is known to activate p53, there was a possibility of cross-talk between Ca^{2+}, p53 and ROS. We therefore measured cellular and nuclear levels of p53 in GaQ_3-treated MCF-7 cells in presence of Ca^{2+} quenching (left panel) and ROS quenching (right panel) over 10 h, using ELISA (Figure 5C). The GaQ_3-induced increase in p53 level and p53 nuclear translocation was abolished by quenching intracellular Ca^{2+} but was unaffected by quenching ROS. The ELISA results were confirmed by immunoprecipitating p53 from the whole cell, nuclear and cytoplasmic fraction of GaQ_3-treated, Ca^{2+} and ROS-quenched MCF-7 cells (Figure 5D). Up-regulation and nuclear translocation of p53 was inhibited after Ca^{2+} quenching, whereas ROS quenching had no effect. These data established that intracellular Ca^{2+} release regulated both p53 and ROS separately, and that intracellular Ca^{2+} release, and not ROS, induced p53 activation in GaQ_3-treated cells.

GaQ_3 induced both FAS-mediated extrinsic and p53-mediated intrinsic apoptosis in cancer cells

As GaQ_3 induced apoptosis in both $p53^{+/+}$ and $p53^{-/-}$ cells, we asked if GaQ_3 might initiate p53-independent extrinsic pathways of apoptosis. Intracellular Ca^{2+} release (Lu and Tian, 2005; Lu *et al.*, 2006; Timmins *et al.*, 2009) increased cellular ROS (Gulbins *et al.*, 1996; Sato *et al.*, 2004; Medan *et al.*, 2005) and p53 was also known to induce and regulate the expression of FAS in cancer cells (Tamura *et al.*, 1995; Bennett *et al.*, 1998; Fukazawa *et al.*, 1999; Sun *et al.*, 2000; Yin *et al.*, 2003; Li *et al.*, 2005b). GaQ_3 induced 67% apoptosis in MCF-7 cells (Figure 6A) and p53 gene silencing significantly reduced the GaQ_3-induced apoptotic fraction (panel 3). This apoptotic fraction was decreased by FAS siRNA (panel 4), suggesting the contribution of an extrinsic apoptotic pathway. Silencing of both p53 and FAS totally prevented GaQ_3-induced apoptosis. Thus both p53-mediated intrinsic, and FAS-mediated extrinsic, pathways of apoptosis were activated by GaQ_3. In $p53^{-/-}$ (H1299) cells (Figure 6B), either Fas silencing (panel 3) or Ca^{2+} quenching (panel 4) abolished GaQ_3-induced apoptosis. These data suggested that, in $p53^{-/-}$ cells, GaQ_3 induced apoptosis only via extrinsic FAS-dependent pathways and that Ca^{2+} was responsible for FAS activation.

To further establish the involvement of FAS in GaQ_3-induced apoptosis, the time course of expression of FAS receptor mRNA and protein was analysed, every 6 h, in GaQ_3-treated MCF-7, H1299 and PC3 cells (Figure 6C) and showed a time-dependent increase in FAS mRNA and protein expression on incubation with GaQ_3. In a parallel experiment, p53 silencing decreased (30%) FAS mRNA expression in GaQ_3-treated MCF-7 cells (Figure 6C, right panel), suggesting that up-regulation of p53 increased FAS gene transcription. Because FAS protein becomes active and induces apoptosis only when it migrates to the cell membrane; we analysed by ELISA the separated cytoplasmic/nuclear and cell membrane fractions of MCF-7, H1299 and PC3 cells (Figures 6D and S19) for FAS. GaQ_3 treatment increased the translocation of FAS from the cytoplasm to the cell membrane in both MCF-7 and H1299 cells. It is also interesting to note that ROS quenching decreased FAS expression in both cell lines, suggesting that Ca^{2+}-induced ROS were also involved in FAS activation.

p53 downstream genes and mir34-a execute apoptosis in GaQ_3-treated cells

GaQ_3 induced apoptosis via both FAS-dependent extrinsic and p53-dependent intrinsic pathways. We therefore analysed the expression of p53 target genes involved in cellular apoptosis. We also analysed the promoter activation and mRNA expression of the p53 regulated family of micro-RNA, mir-34, and its putative role in p53-mediated apoptosis (Raver-Shapira *et al.*, 2007). GaQ_3-treated MCF-7 and H1299 cells were transfected with luciferase constructs carrying mir-34a and mir-34b/c promoter sequences with p53 binding sites (Figure 7A) (He *et al.*, 2007). Only in $p53^{+/+}$ (MCF-7) cells, GaQ_3 induced activity of mir-34a promoter. 18-fold with a 12-fold increase in the mir-34b/c promoter activity. Assays of mir-34a mRNA using real-time PCR, in GaQ_3-treated MCF-7 cells (Figure 7B), showed increased expression, suggesting that mir-34a might play a role in GaQ_3-mediated apoptosis. Western blotting showed that GaQ_3 induced expression of several p53 downstream apoptotic genes, as protein levels of BAX, PUMA, NOXA1, BID, SUMO, p21, APAF1 and PIG3 were significantly higher in GaQ_3-treated MCF-7 cells (Figure 7C).

Discussion

In this study, we have established the mechanisms underlying the anti-neoplastic activity of a novel gallium-derived coordination compound, GaQ_3, that induced both extrinsic and intrinsic pathways of apoptosis. GaQ_3 initiated the intracellular release of Ca^{2+} in $p53^{+/+}$, $p53^{-/-}$ and p53 mutant cell lines, which led to apoptosis. Heavy metals bind to and interact with receptor and intracellular proteins that affect Ca^{2+} homeostasis (Faurskov and Bjerregaard, 2002), and their

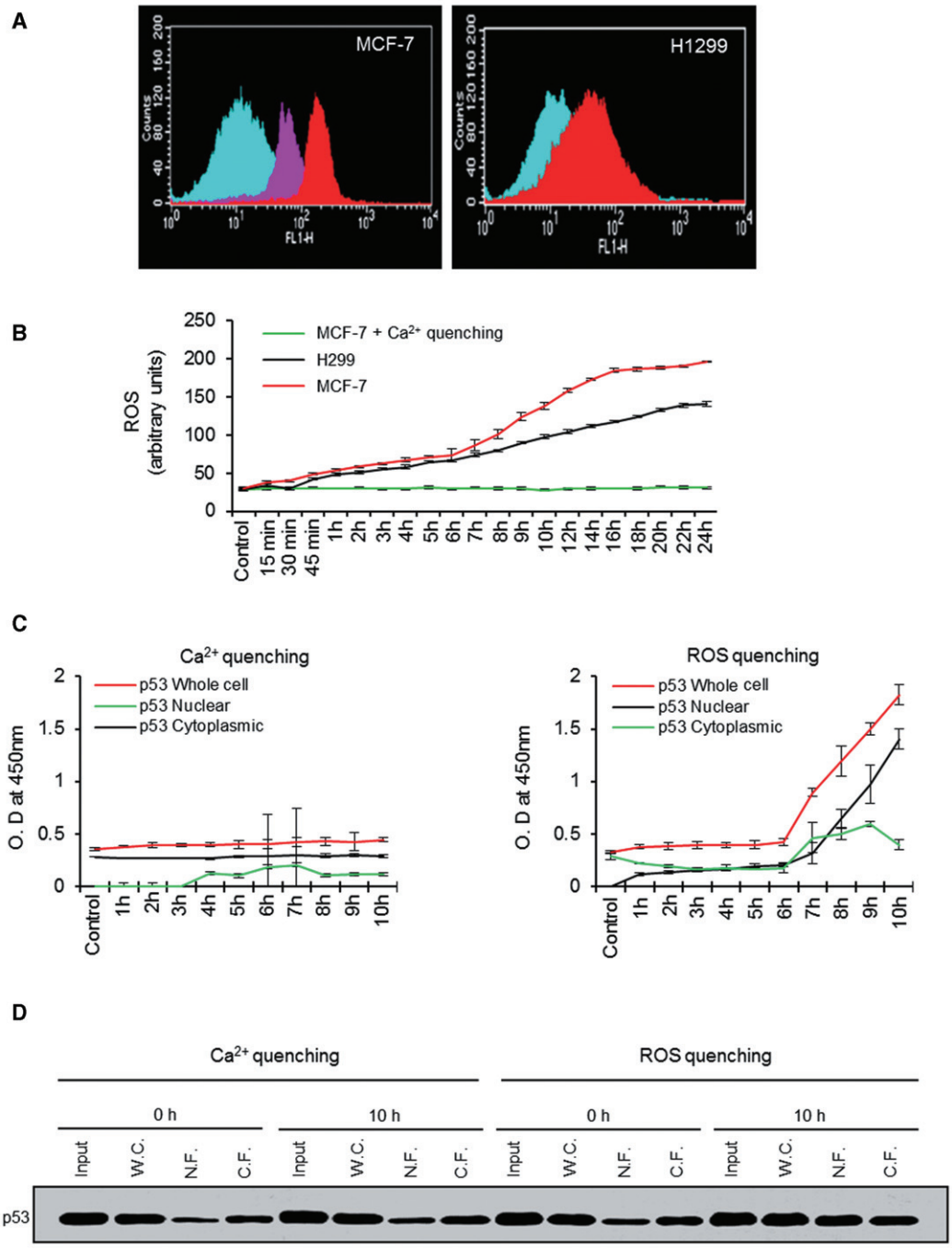

Figure 5

Intracellular Ca^{2+} release induced ROS in GaQ_3-treated cells. (A) Flow cytometry was used to assess ROS generation in GaQ_3-treated MCF-7 and H1299 cells (panels 1 and 2).Results show a significant increase in ROS in both cell lines, and the role of p53 in GaQ_3-induced ROS is confirmed upon silencing p53 gene (blue, untreated cells; red, GaQ_3-treated cells; pink, p53 siRNA in GaQ_3-treated cells). Results show that GaQ_3 induced higher ROS synthesis in $p53^{+/+}$ (MCF-7) cells than in $p53^{-/-}$ (H1299) cells ($n = 7$; Student's t-test). (B) Time-dependent analysis of ROS synthesis, using flow cytometry in GaQ_3-treated MCF-7, GaQ_3-treated H1299 and GaQ_3-treated + Ca^{2+} quenched MCF-7 cells. $p53^{+/+}$ (MCF-7) cells show higher generation of ROS around 7 h of GaQ_3 treatment, than in $p53^{-/-}$ (H1299) cells, which shows a gradual and constant increase in ROS. Ca^{2+} quenching using TMB-8 abolishes GaQ_3-induced ROS, suggesting that ROS generation is dependent on the intracellular Ca^{2+} release ($n = 8$, means ± SD). (C) (Panel i) *In vivo* ELISA shows that quenching of the intracellular Ca^{2+} release using TMB-8 abolishes the p53 protein expression and p53 nuclear translocation in GaQ_3-treated MCF-7 cells. (Panel ii) ROS quenching using N-acetyl cysteine (NAC; 50 μM) shows no change in p53 protein expression and p53 nuclear translocation in GaQ_3-treated MCF-7 cells ($n = 7$, means ± SD). (D) Immunoprecipitation using anti-p53 N terminus (1801Ab) to confirm the results of *in vivo* ELISA. Results (Input, non-immunoprecipitated total protein extract; WC, whole cells; NF, nuclear fraction; CF, cytoplasmic fraction) show that Ca^{2+} quenching, but not ROS quenching using NAC (50 μM), inhibited up-regulation and nuclear translocation of p53 protein at 10 h of GaQ_3 incubation ($n = 5$).

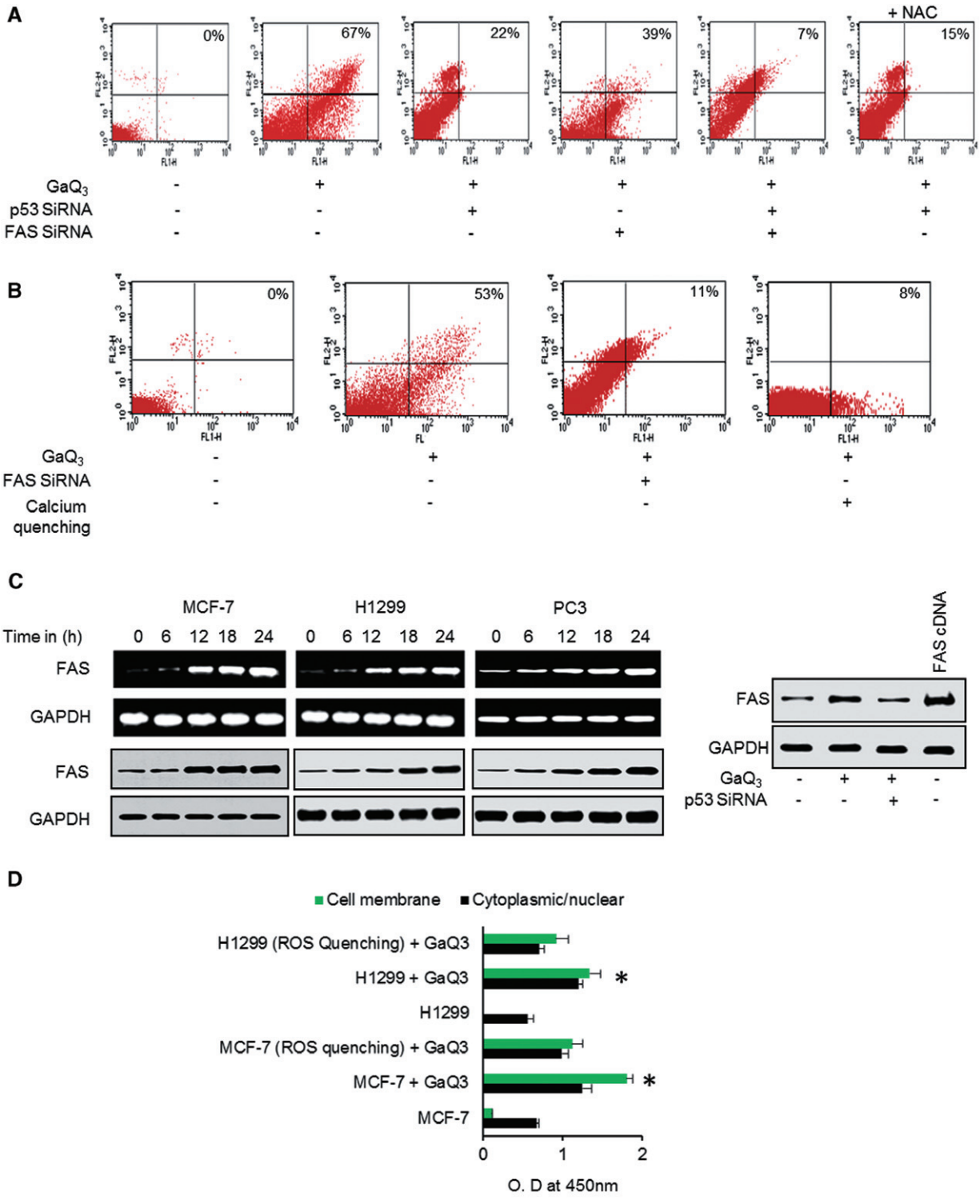

Figure 6

GaQ_3 induces FAS-mediated apoptosis in $p53^{-/-}$ cells. (A) FAS silencing, p53 silencing, Ca^{2+} quenching and combined silencing of p53 and FAS significantly reduced the GaQ_3-induced apoptosis in MCF-7 cells ($n = 10$). (B) Apoptosis was assessed by flow cytometry in GaQ_3-treated H1299 cells with FAS silencing and Ca^{2+} quenching ($n = 10$). (C) (Panel i) RT-PCR to show increased mRNA for FAS receptor in MCF-7, H1299 and PC3 cells treated with GaQ_3 at 0, 6, 12, 18 and 24 h respectively. (Panel ii) Western blot analysis to study expression of FAS protein in MCF-7, H1299 and PC3 cells treated with GaQ_3 for 0, 6, 12, 18 and 24 h respectively. (Panel iii) Western blot to study the role of p53 protein in FAS up-regulation upon silencing p53 in GaQ_3-treated MCF-7 cells ($n = 7$). (D) ELISA of the cell membrane and the nuclear/cytoplasmic fractions of ROS-quenched, GaQ_3-treated MCF-7 and H1299 cells to assess translocation of FAS to the cell membrane. Data shown are means ± SD ($n = 8$). $P < 0.05$, significantly greater than untreated MCF-7 cells or H1299 cells, ANOVA).

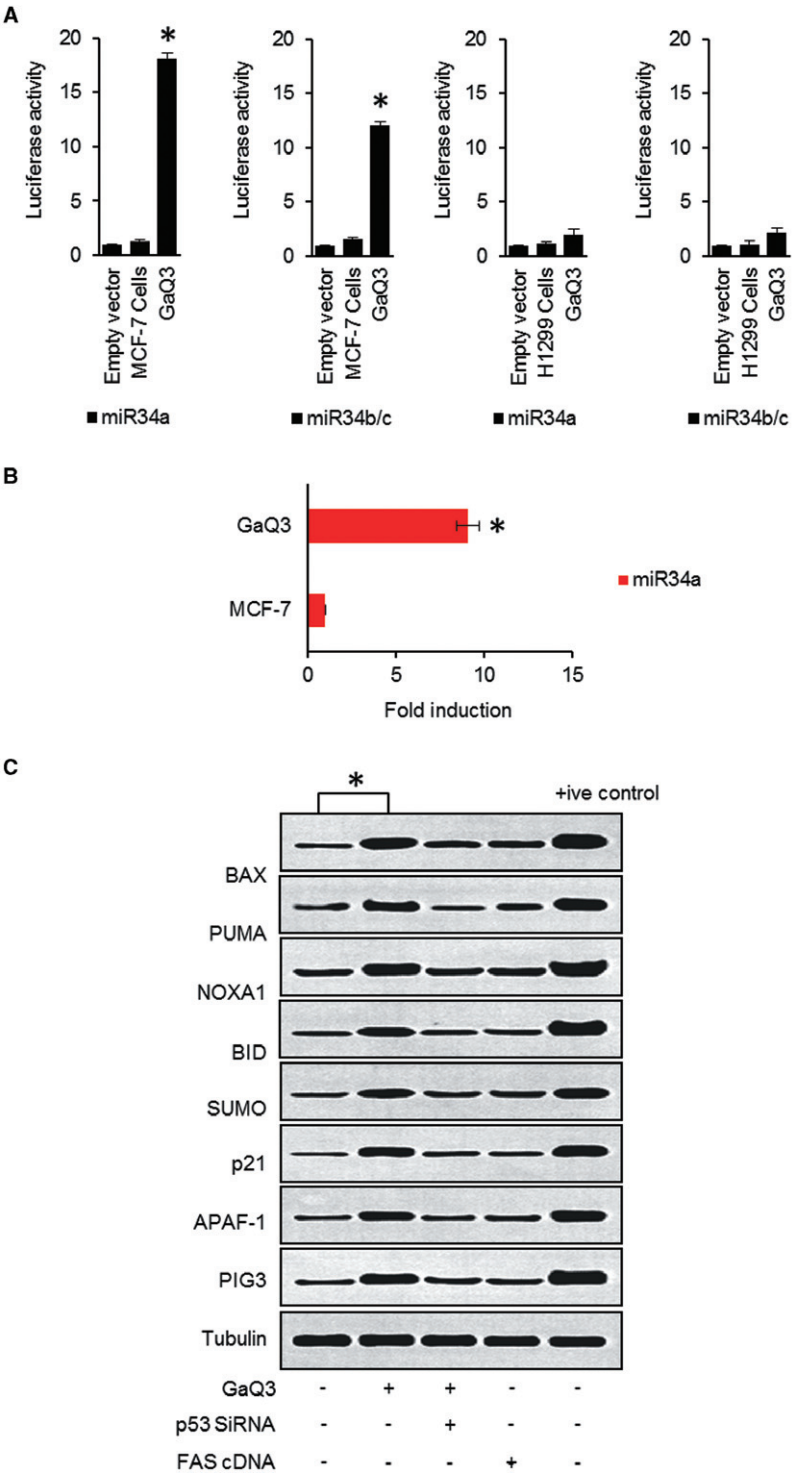

Figure 7

miR-34a was induced and in turn induced the expression of p53 downstream genes involved in apoptosis. (A) Luciferase assay to monitor the mir34a and mir34b/c promoter activity in both untreated and GaQ_3-treated MCF-7 and H1299 cells. Results show a significant increase in both mir-34a and mir34b/c promoter activity only in GaQ_3-treated MCF-7 cells; note that mir-34a activity is higher than mir-34b/c activity (panels 1 and 2). Data shown are means ± SD ($n = 9$); *$P < 0.05$, significant effect of GaQ_3, ANOVA. (B) miR-34a RNA expression quantified in GaQ_3-treated MCF-7 cells using real-time PCR, showed increased miR34a mRNA expression in MCF-7 cells after GaQ_3 (Data shown are means ± SD ($n = 5$); *$P < 0.05$, significant effect of GaQ_3, ANOVA). (C) Western blot analysis shows the up-regulation of p53 downstream genes in GaQ_3-treated MCF-7 cells. The expression of BAX, PUMA, NOXA, BID, SUMO, p21, APAF-1 and PIG3 increased in GaQ_3-treated MCF-7 cells (lane 2), and decreased after p53 silencing (lane 3). Transfection with FAS cDNA shows no effect on the expression of these proteins. The cDNA of all the respective proteins are transfected in the MCF-7 cells and used as positive control. Data shown are means ± SD *$P < 0.05$, significantly different as indicated, ANOVA.

cytotoxicity is known to be related to changes in intracellular Ca^{2+} levels (Lemarie *et al.*, 2004; Wang *et al.*, 2008). Ca^{2+} ions are the cellular messengers that control every aspect of cell and tissue physiology and play a major role in triggering mitotic division in numerous cell types and regulation of cell death (Giorgi *et al.*, 2008). Alterations in the cytoplasmic level of intracellular Ca^{2+} induced apoptosis (McConkey *et al.*, 1992; Berridge, 1993; Orrenius *et al.*, 2003) and Ca^{2+}ions could be turned into death signals when delivered at the wrong time and place (Berridge, 1993; Hajnoczky *et al.*, 2006). Also the transfer of Ca^{2+} from the endoplasmic reticulum (ER) to the mitochondria was required for the initiation of apoptosis. However, some of the Ca^{2+}-induced signals like Ca^{2+}-activated RAF/MEK/ERK pathways also mediate p53-independent apoptosis (Li *et al.*, 2005a).

Our MTT data showed that GaQ_3-mediated cell death occurred in $p53^{+/+}$ (MCF-7 and HepG2), p53 mutant (PC3) and $p53^{-/-}$ (H1299) cells, although in $p53^{+/+}$ cells, GaQ_3 induced apoptosis at lower doses. In $p53^{+/+}$ cells, intracellular Ca^{2+} release stabilized the binding of p53 to its transcriptional co-activator p300 and stabilized the p53 transcriptional complex by recruiting p53–p300 complex to the p53-DNA binding site on the p53 minimal promoter (Tripathi *et al.*, 2007). Ca^{2+} quenching abolished p53–p300 complex formation and the binding of p53–p300 complex to the p53-minimal promoter, suggesting that p53–p300 interaction was Ca^{2+}-dependent. Silencing of p53 or p300 disrupted the p53–p300 complex and its subsequent binding to the p53 minimal promoter. Interestingly, silencing of p53 gene in $p53^{+/+}$ cells switched off intracellular Ca^{2+} release. After 3 h of incubation with GaQ3, p53–p300 complex bound to the p53 minimal promoter. Silencing of p53 or p300 at 3 h abolished the p53–p300 binding to p53 promoter, suggesting that Ca^{2+}-induced formation of the p53–p300 complex was a crucial event in GaQ3-induced p53 activation.

The mechanism of Ca^{2+}–p53 crosstalk is complicated by its different pattern of response to a range of drugs. Patients with p53 deletions have higher serum calcium (Chang *et al.*, 2005). Although both Ca^{2+} binding proteins S100A2 (Mueller *et al.*, 2005) and S100B (Rustandi *et al.*, 2000) bind to the C-terminus of p53, S100A2 increased p53 transcriptional activity, whereas S100B inhibited p53 acetylation in a Ca^{2+}-dependent manner. Furthermore, our data show that in cancer cells, there is a synergistic relation between Ca^{2+} release pattern and status of p53 protein. This conclusion was drawn based upon comparing the intracellular Ca^{2+} release patterns between $p53^{+/+}$ (MCF-7), p53 mutant (PC3) and $p53^{-/-}$ (H1299) cells. In GaQ_3-treated H1299 cells, the release of Ca^{2+} between 0 and 24 h was gradual, whereas in GaQ_3-treated MCF-7 cells, there was a sharp increase in the release of intracellular Ca^{2+} levels at 8 h. This sharp rise in Ca^{2+} was further synchronized with p53 transactivation, as p53 silencing prevented Ca^{2+} release. One then could conclude that Ca^{2+} signalling is responsible for p53 transactivation, leading to p53-dependent apoptosis in cancer cells.

Furthermore, p53 up-regulation was earlier shown to be associated with the generation of ROS (Johnson *et al.*, 1996; Liu *et al.*, 2008). Our data indicated that GaQ_3 induced the generation of ROS in MCF-7, PC3 and H1299 cells, with a slow, gradual and continuous rise in ROS level in $p53^{-/-}$ (H1299) and p53 mutant (PC3) cells, whereas a sudden rise was observed at 9 h in $p53^{+/+}$ (MCF-7) cells. Interestingly, Ca^{2+} quenching reversed ROS generation at 2 h in GaQ_3-treated cells. Intracellular Ca^{2+} release disrupted mitochondrial Ca^{2+} equilibrium, which facilitated the formation of ROS (Lemarie *et al.*, 2004; Wang *et al.*, 2008). In $p53^{-/-}$ cells, GaQ_3-induced Ca^{2+} release must be p53-independent. Thus it was Ca^{2+} and not p53 that was responsible for the generation of ROS. However, in $p53^{+/+}$ cells, Ca^{2+} release up-regulated p53, and this in turn further increased intracellular ROS content at 8 h after GaQ_3 treatment. Our data suggest that Ca^{2+} signalling plays an important role in GaQ_3-induced toxicity, which may also be linked to ROS generation. The cellular redox state could significantly modulate Ca^{2+} signalling (Camello-Almaraz *et al.*, 2006; Davidson and Duchen, 2006; Vercesi *et al.*, 2006; Yan *et al.*, 2006; Zima and Blatter, 2006; Hool and Corry, 2007) and it seems that GaQ_3 initiated a cross-talk between Ca^{2+}-modulated ROS production and ROS-modulated Ca^{2+}-signalling. The anti-cancer drug resveratrol induced an early biphasic increase in the concentration of free intracellular Ca^{2+} in breast cancer cells, probably resulting from depletion of ER Ca^{2+} stores (Sareen *et al.*, 2007). A similar finding was noticed with the anti-cancer agent CDDO which increased cytoplasmic free Ca^{2+} in several cancer cell lines. A Ca^{2+} chelator reduced CDDO-induced increase in cytoplasmic free Ca^{2+} inhibiting caspase activation and DNA fragmentation, implying that Ca^{2+} played a pivotal role in signalling the initiation of apoptosis (Hail *et al.*, 2004). By contrast a calcium mobilizer, calcimycin, activated the RAF/MEK/ERK pathway through RAS, which was essential for the induction of apoptosis (Li *et al.*, 2005a).

GaQ_3 activated mir34 a/b/c promoters, exclusively, in $p53^{+/+}$ MCF-7 cells, shown by the more than eight-fold rise in mRNA levels. A member of the miRNA34 family, miR-34a, which is commonly deleted in human cancers, is directly trans-activated by p53. Expression of miR-34a causes dramatic reprogramming of gene expression and promotes apoptosis. Therefore, it is likely that an important function of miR-34a is the modulation and fine-tuning of the gene expression program initiated by p53 (Chang *et al.*, 2007; Hermeking, 2007). As p53 induces over-expression of miR-34a, it is a direct pro-apoptotic transcriptional target of p53 that can mediate some of the biological effects of p53 (Raver-Shapira *et al.*, 2007).

Ca^{2+} signalling also activates the FAS-mediated pathway of cell death (Zhang *et al.*, 2010)and FAS up-regulation as well as its translocation to the cell membrane causes apoptosis (Nagata, 1996). The fact that GaQ_3 up-regulated FAS in MCF-7, PC3 and H1299 cells further confirmed that the GaQ_3-mediated apoptotic cell death may be due to p53-dependent (intrinsic) and p53-independent (extrinsic) pathways. Strikingly, cisplatin-induced apoptosis, which was associated with p53-dependent and -independent responses, was also reported in human bladder cancer cells (Konstantakou *et al.*, 2009), and both intrinsic and extrinsic pathways were observed in TNF-α induced apoptosis, which was further enhanced in presence of cisplatin (Barton *et al.*, 2005). However, cisplatin exclusively induced intrinsic apoptosis in inner ear cells (Garcia-Berrocal *et al.*, 2007). By contrast, bleomycin induced only the extrinsic pathway in pulmonary endothelial cells (Mungunsukh *et al.*, 2010).

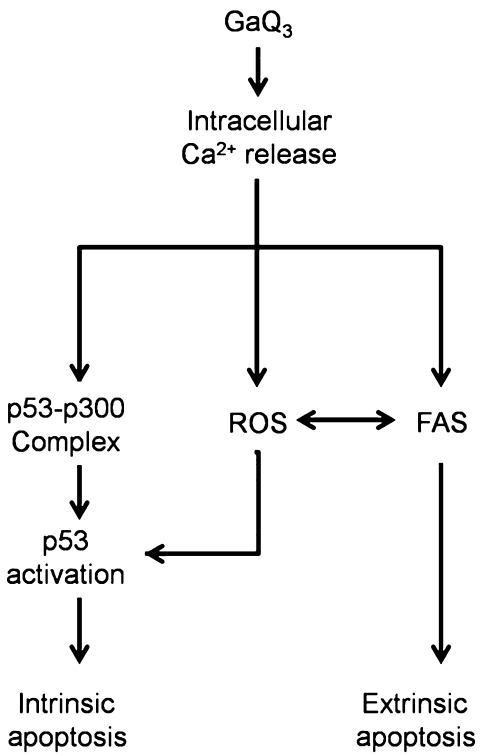

Figure 8

Scheme outlining the mechanisms involved in the action of GaQ_3 in cancer cells.

In conclusion, we have established the mechanism of action of a novel anti-cancer gallium complex GaQ_3 in a variety of cancer cells with different p53 status. A model has been proposed to explain the mechanism of GaQ_3-induced apoptosis in cancer cells (Figure 8). GaQ_3-mediated intracellular Ca^{2+} release is the primary event that triggers both p53-dependent intrinsic and p53-independent extrinsic apoptosis. A future strategy would be to explore the complex nature of p53–Ca^{+2} cross-talk, with reference to GaQ_3-induced apoptosis.

Acknowledgement

This research work is funded by the Jawaharlal Nehru University LRE grant year 2010.

Conflict of interest

None of the authors have any conflict of interest in this study.

References

Barton C, Davies D, Balkwill F, Burke F (2005). Involvement of both intrinsic and extrinsic pathways in IFN-gamma-induced apoptosis that are enhanced with cisplatin. Eur J Cancer 41: 1474–1486.

Bennett M, Macdonald K, Chan SW, Luzio JP, Simari R, Weissberg P (1998). Cell surface trafficking of Fas: a rapid mechanism of p53-mediated apoptosis. Science 282: 290–293.

Berridge MJ (1993). Inositol trisphosphate and calcium signalling. Nature 361: 315–325.

Camello-Almaraz C, Gomez-Pinilla PJ, Pozo MJ, Camello PJ (2006). Mitochondrial reactive oxygen species and Ca2+ signaling. Am J Physiol Cell Physiol 291: C1082–C1088.

Campaner S, Spreafico F, Burgold T, Doni M, Rosato U, Amati B *et al.* (2011). The Methyltransferase Set7/9 (Setd7) Is Dispensable for the p53-Mediated DNA Damage Response In Vivo. Mol Cell 43: 681–688.

Chang H, Qi C, Yi QL, Reece D, Stewart AK (2005). p53 gene deletion detected by fluorescence in situ hybridization is an adverse prognostic factor for patients with multiple myeloma following autologous stem cell transplantation. Blood 105: 358–360. (new ref).

Chang TC, Wentzel EA, Kent OA, Ramachandran K, Mullendore M, Lee KH *et al.* (2007). Transactivation of miR-34a by p53 broadly influences gene expression and promotes apoptosis. Mol Cell 26: 745–752. (new ref).

Chen D, Frezza M, Shakya R, Cui QC, Milacic V, Verani CN *et al.* (2007). Inhibition of the proteasome activity by gallium(III) complexes contributes to their anti prostate tumor effects. Cancer Res 67: 9258–9265.

Chitambar CR (2004). Gallium compounds as antineoplastic agents. Curr Opin Oncol 16: 547–552.

Chitambar CR, Wereley JP, Heiman T, Antholine WE, O'Brien WJ (2000). Cellular adaptation to down-regulated iron transport into lymphoid leukaemic cells: effects on the expression of the gene for ribonucleotide reductase. Biochem J 345: 681–685.

Chitambar CR, Purpi DP, Woodliff J, Yang M, Wereley JP (2007). Development of gallium compounds for treatment of lymphoma: gallium maltolate, a novel hydroxypyrone gallium compound, induces apoptosis and circumvents lymphoma cell resistance to gallium nitrate. J Pharmacol Exp Ther 322: 1228–1236.

Davidson SM, Duchen MR (2006). Calcium microdomains and oxidative stress. Cell Calcium 40: 561–574.

Desaint S, Luriau S, Aude JC, Rousselet G, Toledano MB (2004). Mammalian antioxidant defenses are not inducible by H2O2. J Biol Chem 279: 31157–31163.

Einhorn L (2003). Gallium nitrate in the treatment of bladder cancer. Semin Oncol 30 (Suppl. 5): 34–41.

Faurskov B, Bjerregaard HF (2002). Evidence for cadmium mobilization of intracellular calcium through a divalent cation receptor in renal distal epithelial A6 cells. Pflugers Arch 445: 40–50.

Fukazawa T, Fujiwara T, Morimoto Y, Shao J, Nishizaki M, Kadowaki Y *et al.* (1999). Differential involvement of the CD95 (Fas/APO-1) receptor/ligand system on apoptosis induced by the wild-type p53 gene transfer in human cancer cells. Oncogene 18: 2189–2199.

Garcia-Berrocal JR, Nevado J, Ramirez-Camacho R, Sanz R, Gonzalez-Garcia JA, Sanchez-Rodriguez C *et al.* (2007). The anticancer drug cisplatin induces an intrinsic apoptotic pathway inside the inner ear. Br J Pharmacol 152: 1012–1020.

Giorgi C, Romagnoli A, Pinton P, Rizzuto R (2008). Ca2+ signaling, mitochondria and cell death. Curr Mol Med 8: 119–130.

Gulbins E, Brenner B, Schlottmann K, Welsch J, Heinle H, Koppenhoefer U *et al.* (1996). Fas-induced programmed cell death is mediated by a Ras-regulated O2- synthesis. Immunology 89: 205–212.

Hail N Jr, Konopleva M, Sporn M, Lotan R, Andreeff M (2004). Evidence supporting a role for calcium in apoptosis induction by the synthetic triterpenoid 2-cyano-3,12-dioxooleana-1,9-dien-28-oic acid (CDDO). J Biol Chem 279: 11179–11187.

Hajnoczky G, Csordas G, Das S, Garcia-Perez C, Saotome M, Sinha Roy S *et al.* (2006). Mitochondrial calcium signalling and cell death: approaches for assessing the role of mitochondrial Ca2+ uptake in apoptosis. Cell Calcium 40: 553–560.

He L, He X, Lim LP, de Stanchina E, Xuan Z, Liang Y *et al.* (2007). A microRNA component of the p53 tumour suppressor network. Nature 447: 1130–1134.

Hermeking H (2007). p53 enters the microRNA world. Cancer Cell 12: 414–418. (new ref).

Hool LC, Corry B (2007). Redox control of calcium channels: from mechanisms to therapeutic opportunities. Antioxid Redox Signal 9: 409–435.

Ikura M, Yap KL (2000). Where cancer meets calcium–p53 crosstalk with EF-hands. Nat Struct Biol 7: 525–527.

Jakupec MA, Keppler BK (2004). Gallium and other main group metal compounds as antitumor agents. Met Ions Biol Syst 42: 425–462.

Johnson TM, Yu ZX, Ferrans VJ, Lowenstein RA, Finkel T (1996). Reactive oxygen species are downstream mediators of p53-dependent apoptosis. Proc Natl Acad Sci U S A 93: 11848–11852.

Joseph TP, Janine PW, Chitambar CR (2005). Gallium nitrate as a novel agent for the treatment of mantle cell lymphoma: Target and mechanisms of action. Proc Am Assoc Cancer Res 46: 1383–1384.

Konstantakou EG, Voutsinas GE, Karkoulis PK, Aravantinos G, Margaritis LH, Stravopodis DJ (2009). Human bladder cancer cells undergo cisplatin-induced apoptosis that is associated with p53-dependent and p53-independent responses. Int J Oncol 35: 401–416.

Kowaltowski AJ, Naia-da-Silva ES, Castilho RF, Vercesi AE (1998). Ca2+-stimulated mitochondrial reactive oxygen species generation and permeability transition are inhibited by dibucaine or Mg2+. Arch Biochem Biophys 359: 77–81.

Lemarie A, Lagadic-Gossmann D, Morzadec C, Allain N, Fardel O, Vernhet L (2004). Cadmium induces caspase-independent apoptosis in liver Hep3B cells: role for calcium in signaling oxidative stress-related impairment of mitochondria and relocation of endonuclease G and apoptosis-inducing factor. Free Radic Biol Med 36: 1517–1531.

Li DW, Liu JP, Mao YW, Xiang H, Wang J, Ma WY *et al.* (2005a). Calcium-activated RAF/MEK/ERK signaling pathway mediates p53-dependent apoptosis and is abrogated by alpha B-crystallin through inhibition of RAS activation. Mol Biol Cell 16: 4437–4453.

Li Y, Mao Y, Rosal RV, Dinnen RD, Williams AC, Brandt-Rauf PW *et al.* (2005b). Selective induction of apoptosis through the FADD/caspase-8 pathway by a p53 c-terminal peptide in human pre-malignant and malignant cells. Int J Cancer 115: 55–64.

Liu B, Chen Y, St Clair DK (2008). ROS and p53: a versatile partnership. Free Radic Biol Med 44: 1529–1535.

Lu B, Wang L, Stehlik C, Medan D, Huang C, Hu S *et al.* (2006). Phosphatidylinositol 3-kinase/Akt positively regulates Fas (CD95)-mediated apoptosis in epidermal Cl41 cells. J Immunol 176: 6785–6793.

Lu QP, Tian L (2005). Fas mRNA expression and calcium influx change in H2O2-induced apoptotic hepatocytes in vitro. World J Gastroenterol 11: 534–537.

McConkey DJ, Jondal M, Orrenius S (1992). Cellular signaling in thymocyte apoptosis. Semin Immunol 4: 371–377.

Medan D, Wang L, Toledo D, Lu B, Stehlik C, Jiang BH *et al.* (2005). Regulation of Fas (CD95)-induced apoptotic and necrotic cell death by reactive oxygen species in macrophages. J Cell Physiol 203: 78–84.

Mendes IC, Soares MA, Dos Santos RG, Pinheiro C, Beraldo H (2009). Gallium(III) complexes of 2-pyridineformamide thiosemicarbazones: cytotoxic activity against malignant glioblastoma. Eur J Med Chem 44: 1870–1877.

Mueller A, Schafer BW, Ferrari S, Weibel M, Makek M, Hochli M *et al.* (2005). The calcium-binding protein S100A2 interacts with p53 and modulates its transcriptional activity. J Biol Chem 280: 29186–29193. (new ref).

Muller M, Strand S, Hug H, Heinemann EM, Walczak H, Hofmann WJ *et al.* (1997). Drug-induced apoptosis in hepatoma cells is mediated by the CD95 (APO-1/Fas) receptor/ligand system and involves activation of wild-type p53. J Clin Invest 99: 403–413.

Mungunsukh O, Griffin AJ, Lee YH, Day RM (2010). Bleomycin induces the extrinsic apoptotic pathway in pulmonary endothelial cells. Am J Physiol Lung Cell Mol Physiol 298: L696–L703.

Nagata S (1996). Fas-induced apoptosis, and diseases caused by its abnormality. Genes Cells 1: 873–879.

Orrenius S, Zhivotovsky B, Nicotera P (2003). Regulation of cell death: the calcium-apoptosis link. Nat Rev Mol Cell Biol 4: 552–565.

Raver-Shapira N, Marciano E, Meiri E, Spector Y, Rosenfeld N, Moskovits N *et al.* (2007). Transcriptional activation of miR-34a contributes to p53-mediated apoptosis. Mol Cell 26: 731–743.

Rustandi RR, Baldisseri DM, Weber DJ (2000). Structure of the negative regulatory domain of p53 bound to S100B(betabeta). Nat Struct Biol 7: 570–574. (new ref).

Sareen D, Darjatmoko SR, Albert DM, Polans AS (2007). Mitochondria, calcium, and calpain are key mediators of resveratrol-induced apoptosis in breast cancer. Mol Pharmacol 72: 1466–1475.

Sato T, Machida T, Takahashi S, Iyama S, Sato Y, Kuribayashi K *et al.* (2004). Fas-mediated apoptosome formation is dependent on reactive oxygen species derived from mitochondrial permeability transition in Jurkat cells. J Immunol 173: 285–296.

Sheard MA, Vojtesek B, Janakova L, Kovarik J, Zaloudik J (1997). Up-regulation of Fas (CD95) in human p53wild-type cancer cells treated with ionizing radiation. Int J Cancer 73: 757–762.

Son YO, Lee JC, Hitron JA, Pan J, Zhang Z, Shi X (2010). Cadmium induces intracellular Ca2+- and H2O2-dependent apoptosis through JNK- and p53-mediated pathways in skin epidermal cell line. Toxicol Sci 113: 127–137.

Straus DJ (2003). Gallium nitrate in the treatment of lymphoma. Semin Oncol 30 (Suppl. 5): 25–33.

Sun SY, Yue P, Hong WK, Lotan R (2000). Induction of Fas expression and augmentation of Fas/Fas ligand-mediated apoptosis by the synthetic retinoid CD437 in human lung cancer cells. Cancer Res 60: 6537–6543.

Takemura H, Hughes AR, Thastrup O, Putney JW Jr (1989). Activation of calcium entry by the tumor promoter thapsigargin in parotid acinar cells. Evidence that an intracellular calcium pool and not an inositol phosphate regulates calcium fluxes at the plasma membrane. J Biol Chem 264: 12266–12271.

Tamura T, Aoyama N, Saya H, Haga H, Futami S, Miyamoto M *et al.* (1995). Induction of Fas-mediated apoptosis in p53-transfected human colon carcinoma cells. Oncogene 11: 1939–1946.

Timmins JM, Ozcan L, Seimon TA, Li G, Malagelada C, Backs J *et al.* (2009). Calcium/calmodulin-dependent protein kinase II links ER stress with Fas and mitochondrial apoptosis pathways. J Clin Invest 119: 2925–2941.

Tripathi V, Ali A, Bhat R, Pati U (2007). CHIP chaperones wild type p53 tumor suppressor protein. J Biol Chem 282: 28441–28454.

Valiahdi SM, Heffeter P, Jakupec MA, Marculescu R, Berger W, Rappersberger K *et al.* (2009). The gallium complex KP46 exerts strong activity against primary explanted melanoma cells and induces apoptosis in melanoma cell lines. Melanoma Res 19: 283–293.

Vercesi AE, Kowaltowski AJ, Oliveira HC, Castilho RF (2006). Mitochondrial Ca2+ transport, permeability transition and oxidative stress in cell death: implications in cardiotoxicity, neurodegeneration and dyslipidemias. Front Biosci 11: 2554–2564.

Wang L, Azad N, Kongkaneramit L, Chen F, Lu Y, Jiang BH *et al.* (2008). The Fas death signaling pathway connecting reactive oxygen species generation and FLICE inhibitory protein down-regulation. J Immunol 180: 3072–3080.

Yamagami K, Nishimura S, Sorimachi M (1998). Cd2+ and Co2+ at micromolar concentrations mobilize intracellular Ca2+ via the generation of inositol 1,4,5-triphosphate in bovine chromaffin cells. Brain Res 798: 316–319.

Yan Y, Wei CL, Zhang WR, Cheng HP, Liu J (2006). Cross-talk between calcium and reactive oxygen species signaling. Acta Pharmacol Sin 27: 821–826.

Yin Y, Liu YX, Jin YJ, Hall EJ, Barrett JC (2003). PAC1 phosphatase is a transcription target of p53 in signalling apoptosis and growth suppression. Nature 422: 527–531.

Zanias S, Papaefstathiou GS, Raptopoulou CP, Papazisis KT, Vala V, Zambouli D *et al.* (2010). Synthesis, structure, and antiproliferative activity of three gallium(III) azole complexes. Bioinorg Chem Appl doi: 10.1155/2010/168030.

Zhang F, Xia M, Li PL (2010). Lysosome-dependent Ca(2+) release response to Fas activation in coronary arterial myocytes through NAADP: evidence from CD38 gene knockouts. Am J Physiol Cell Physiol 298: C1209–C1216.

Zhang W, Couldwell WT, Song H, Takano T, Lin JH, Nedergaard M (2000). Tamoxifen-induced enhancement of calcium signaling in glioma and MCF-7 breast cancer cells. Cancer Res 60: 5395–5400.

Zhao Y, Chaiswing L, Velez JM, Batinic-Haberle I, Colburn NH, Oberley TD *et al.* (2005). p53 translocation to mitochondria precedes its nuclear translocation and targets mitochondrial oxidative defense protein-manganese superoxide dismutase. Cancer Res 65: 3745–3750.

Zima AV, Blatter LA (2006). Redox regulation of cardiac calcium channels and transporters. Cardiovasc Res 71: 310–321.

Supporting information

Additional Supporting Information may be found in the online version of this article:

Figure S1 MTT assay in MCF-7 cells ($p53^{+/+}$) treated with GaQ3 for 0, 24, 48 and 72 h. All the cells are treated with dose of GaQ3 varying from 1 to 10 μM (n = 10, mean; SD, statistical analysis; ANOVA).

Figure S2 MTT assay in HepG2 cells ($p53^{+/+}$) treated with GaQ3 for 0, 24, 48 and 72 h. All the cells are treated with dose of GaQ3 varying from 1 to 10 μM (n = 10, mean; SD, statistical analysis; ANOVA).

Figure S3 MTT assay in PC3 cells (p53 mutant) treated with GaQ3 for 0, 24, 48 and 72 h. All the cells are treated with dose of GaQ3 varying from 1 to 10 μM (n = 10, mean; SD, statistical analysis; ANOVA).

Figure S4 MTT assay in H1299 cells ($p53^{-/-}$) treated with GaQ3 for 0, 24, 48 and 72 h. All the cells are treated with dose of GaQ3 varying from 1 to 10 μM (n = 10, mean; SD, statistical analysis; ANOVA).

Figure S5 MTT assay in GaQ3-treated $p53^{+/+}$ (MCF-7 and HepG2), $p53^{-/-}$ (H1299) and p53 mutant (PC3) cells. All the cells are treated for 24 h with doses of GaQ3 varying from 1 to 10 μM (n = 10, mean; SD, statistical analysis; ANOVA).

Figure S6 LDH assay in GaQ3-treated $p53^{+/+}$ (MCF-7 and HepG2), $p53^{-/-}$ (H1299) and p53 mutant (PC3) cells. All the cells are treated for 24 h with dose of GaQ3 varying from 1 to 10 μM (n = 10, mean; SD, statistical analysis; ANOVA).

Figure S7 Cell cycle distribution curve of GaQ3-treated PC3 cells (p53 mutant) was analysed using flow cytometry. Results show that GaQ3 induces G_0–G_1 phase arrest in PC3 cells (n = 7). Lower panel: the cell cycle distribution curves of GaQ3-treated MCF-7, H1299 and PC3 cell are graphically represented (n = 5, mean; SD, statistical analysis; ANOVA).

Figure S8 Percentage cellular apoptosis in GaQ3-treated MCF-7, H1299 and PC3 cells was measured using Annexin V staining and flow cytometry (n = 8, error bars; SD, statistical analysis; ANOVA).

Figure S9 Percentage cellular apoptosis was measured in GaQ3 + DEVD-FMK (caspase inhibitor) treated MCF-7 cells using Annexin V staining and flow cytometry. Results show a significant decrease in GaQ3-induced apoptosis upon incubation with DEVD-FMK (n = 10, mean; SD, statistical analysis; ANOVA).

Figure S10 TUNEL staining shows cellular apoptosis in PC3 cells upon GaQ3 treatment (n = 4). Lower panel: percentage TUNEL-positive cells are shown in GaQ3-treated MCF-7, H1299 and PC3 cells (n = 10, mean; SD, statistical analysis; ANOVA).

Figure S11 p53 2.5 Kb promoter activity was measured using luciferase assay, in GaQ3-treated MCF-7 cells in which intracellular calcium release is quenched using TMB-8. Results show that p53 promoter is inactive upon calcium quenching (n = 7, mean; SD, statistical analysis; ANOVA).

Figure S12 p53 minimal promoter activity was measured using luciferase assay, in GaQ3-treated MCF-7 cells in which p300 gene is silenced using p300 siRNA. Results show that p53 minimal promoter is inactive in absence of p300 (n = 7, mean; SD, statistical analysis; ANOVA).

Figure S13 p53 mRNA analysis (time course) in GaQ3-treated MCF-7 cells and TMB-8 + GaQ3-treated MCF-7 cells (calcium quenching), using real-time PCR. Results show that the GaQ3-induced 6 h rise in p53 mRNA level is abolished upon calcium quenching (n = 6, mean; SD, statistical analysis; ANOVA).

Figure S14 p53 mRNA analysis using real-time PCR shows that p300 siRNA abolished the GaQ3-induced rise in p53 mRNA level (lane 5). This data suggest the crucial role of p53–p300 complex in p53 mRNA synthesis (n = 5, mean; SD, statistical analysis; ANOVA). Lower panel: the role of p300 in p53 protein synthesis is observed. GaQ3-induced rise in p53 protein level (lane 2) is reversed upon p300 gene silencing (lane 3) in MCF-7 cells (n = 4).

Figure S15 Immunoprecipitation experiment shows the separation of the nuclear and cytoplasmic fractions of the MCF-7 cells. Immunoprecipitation (IPP) with PARP antibody only stains the nuclear fraction and not the cytoplasmic fractions, and IPP with tubulin antibody stains only the cytoplasmic fractions. The non-immunoprecipitated total protein extracts (Input) are used as controls (n = 4).

Figure S16 Time-dependent analysis of GaQ3-induced DNA damage is conducted in MCF-7 cells. Results show that GaQ3 does not induce DNA damage until 15 h incubation with MCF-7 cells (n = 11, mean; SD, statistical analysis; ANOVA). Lower panel: GaQ3-induced cellular DNA damage is analysed in PC3 and H1299 cells (n = 9, mean; SD, statistical analysis; ANOVA).

Figure S17 The rise in cellular ROS is observed in GaQ3-treated H1299 cells using DCHF-DA staining in flow cytometry (n = 7).

Figure S18 Time-dependent analysis of GaQ3-induced rise in cellular ROS was measured in PC3 cells using flow cytometry. Results show that GaQ3 induces constant increase in the cellular ROS (red line). Upon quenching intracellular calcium release using TMB-8, the GaQ3-induced rise in cellular ROS is abolished (black line) (n = 11, mean; SD, statistical analysis; ANOVA).

Figure S19 ELISA of the cell membrane (green) and the nuclear/cytoplasmic (black) fractions of ROS quenched, GaQ3-treated PC3 cells was performed to examine the translocation of FAS on the cell membrane (n = 8, mean; SD, statistical analysis; ANOVA).